LASER & PHOTONICS REVIEWS
www.lpr-journal.org

# Recent Progress of Supercontinuum Generation in Nanophotonic Waveguides

*Yuxi Fang, Changjing Bao, Si-Ao Li, Zhi Wang, Wenpu Geng, Yingning Wang, Xu Han, Jicong Jiang, Weigang Zhang, Zhongqi Pan, Zhaohui Li, and Yang Yue**

**Supercontinuum (SC) has opened up possibilities for numerous applications in optical communications, signal processing, metrology, and spectroscopy. Supercontinuum generation (SCG) in the integrated nonlinear platforms has attracted much interest recently, due to its fundamental advantages in terms of complementary metal oxide semiconductor compatibility, low power consumption, compact size, and cost-effectiveness. In this paper, the latest progress on various types of nanophotonic waveguides for SCG is reviewed. The material properties of silicon, germanium, silicon–germanium alloy, silicon nitride, silica, chalcogenide, III–V materials, lithium niobate, and other materials, which are used as nonlinear media for SCG are discussed. The wavelength-dependent nonlinear Kerr index, material, and nonlinear loss of the waveguides are taken into account. This review mainly focuses on the SCG resulting from the cubic $\chi^{(3)}$ nonlinearity processes pumped by the femtosecond pulse. The recent representative SCG works based on the integrated optical waveguides are summarized, and further classified according to the dispersion characteristics. Furthermore, different types of spectra broadening mechanisms in details according to the classifications are analyzed. Perspectives on the SC spectral coverage, the realization of various dispersion curves, and the novel materials, which are the key aspects of the SCG in nanophotonic waveguides are provided.**

## 1. Introduction

Optical nonlinear effects including second-harmonic generation (SHG),[1–3] third-harmonic generation (THG),[4–7] self-phase modulation (SPM),[8–12] cross-phase modulation,[13–15] stimulated Raman scattering (SRS),[16–20] and four-wave mixing (FWM),[18,21–24] have been discovered and explored over the past century, and they are widely used for various applications. All of these nonlinear effects are being explored to realize a variety of optical applications on the chip scale.[25,26] The optical nonlinear functions, such as the wavelength conversion,[27–31] parametric gain,[32,33] soliton and pulse compression,[34–37] supercontinuum generation (SCG),[38] and frequency comb generation[39–41] have been widely demonstrated in recent years. In particular, SCG is one of the most important nonlinear optical phenomena. Due to the interaction of the nonlinear effects and chromatic dispersion (CD), the optical spectrum of an input pulse could be broadened over a frequency range exceeding 100 THz.[42] This extremely spectral broadening is referred as SCG. In other words, as an optical pulse propagates through a highly nonlinear media, new frequency components can be generated during the nonlinear process, which is also affected by the dispersion and loss properties of the media. Choosing media with large nonlinearity and small loss, engineering its overall CD by waveguide dispersion adjustment, and selecting a suitable injection pulse are the critical directions for SCG. In addition, the bandwidth, coherence, and flatness are the key factors to characterize the supercontinuum (SC) source, which could be seen as a criterion to evaluate the SC.

SCG has been demonstrated as a key enabling technology for many potential applications,[43,44] optical coherence tomography,[43–46] high-precision frequency metrology,[47] molecular spectroscopy,[48–50] and biological,[51–53] chemical,[54,55]

Y. Fang, S.-A. Li, Z. Wang, W. Geng, Y. Wang, X. Han, J. Jiang, W. Zhang
Institute of Modern Optics
Nankai University
Tianjin 300350, China

C. Bao
Department of Electrical Engineering
University of Southern California
Los Angeles 90089, USA

Z. Pan
Department of Electrical & Computer Engineering
University of Louisiana at Lafayette
Lafayette 70504, USA

Z. Li
State Key Laboratory of Optoelectronic Materials and Technologies
School of Electronics and Information Technology
Sun Yat-sen University
Guangzhou 510275, China

Y. Yue
School of Information and Communications Engineering
Xi'an Jiaotong University
Xi'an 710049, China
E-mail: yueyang@xjtu.edu.cn

The ORCID identification number(s) for the author(s) of this article can be found under https://doi.org/10.1002/lpor.202200205

**DOI: 10.1002/lpor.202200205**

environmental[56,57] sensing. Furthermore, the sliced SC spectra could be used for wavelength division multiplexing applications in optical communications systems.[58–60] Some emerging applications, such as Lidar, also consider to utilize the SC source to reflect the spectral intensity information of the target.[61] Some applications also demonstrate the importance of the spectrum coherence. For example, precision frequency metrology or molecular spectroscopy require highly coherent SC source, which features little pulse-to-pulse variations and timing jitter.[62]

SC was first reported in bulk glass in 1970s,[63,62] and the SC generation in photonic crystal fibers attracted widespread interests in the late 1990s,[64] and still has been an area of active research over the past decade.[65] Broadband SCG has been demonstrated in microstructure fibers[59,66–70] and high nonlinear fibers.[71–73] Compared with fibers, the integrated nonlinear platforms offer the desirable features for the SCG, which include the advantages of high effective nonlinearities, small footprint, and low energy consumption. In some application scenarios, it is highly desirable to achieve coherent SC in a compact cost-effective and power efficient manner. Integrated photonics is one of the most promising solutions. Silicon (Si),[25,74–78] germanium (Ge),[79–82] the silicon germanium (SiGe) alloy,[83–86] silicon nitride ($Si_3N_4$),[87–92] silica ($SiO_2$),[93–97] chalcogenide,[98–103] III–V materials,[104–107] lithium niobate ($LiNbO_3$),[108–110] and other materials[111–114] play the important roles in chip-scale nonlinear applications. Among the above waveguide materials, silicon-on-insulator (SOI) has led this field for several years due to its high refractive index and high Kerr nonlinearity inherently.[115–120] However, Si suffers from the two-photon absorption (TPA) induced significant nonlinear absorption in the telecommunication band,[116,121–124] which further limits its applications. This requirement provides the opportunity for other nonlinear platforms, which have significantly low nonlinear loss and could be potential for future all-optical photonic chip applications.

In addition to the nonlinearity, dispersion engineering is another key factor to achieve the broadband nonlinear functions. The material dispersion of the typical materials used in the nanophotonic waveguides is given in Section 2.2, and the waveguide dispersion is determined by the geometric parameters of the waveguides. Specially, compared with the strip waveguide, novel waveguiding structures[125–134] including the slot waveguide[25,128–134] could provide more freedoms for waveguide dispersion engineering. There are several main design targets for the overall CD engineering: CD with multiple zero-dispersion wavelengths (ZDWs), which could provide ideal phase-matching condition and large conversion efficiency in the nonlinear parametric processes;[42,127,128,135–138] broadband flattened CD, which could be used to realize the dispersion compensation over a broad band in the communication systems.

In this paper, we review the SCG in various existing integrated photonics platforms and classify these demonstrations according to the spectral broadening mechanisms. The rest of the paper is organized as follows: In Section 2, we discuss and compare the material characteristics including loss, dispersion, and nonlinearity, which determine the performance of SCG. This section provides the reference for material choices in nonlinear photonics applications. In Section 3, the fundamental equations of the nonlinear propagation and the spectral coherence are discussed. Section 5 reviews the SCG from the third-order nonlinearity process in details and is grouped into two categories in terms of the injected pulse duration, the regime using longer picosecond or continuous-wave (CW) pump and the femtosecond regime pump. We introduce the femtosecond regime in more details because it forms the particularly dynamic mechanism in the SCG processes, which is the basis of spectral broadening in most researches. We summarize various waveguide structures and the material combination between the high-index core and the low-index cladding, and discuss the features of multi-stage waveguides. We also review the existing SC experimental results based on different integrated materials, and further compare them in order to obtain the commonly used experiment method in practice and the corresponding broadband spectra. In order to illustrate the physical mechanisms involved in SCG, we attempt to classify the SCG process in terms of the key factor, that is, the dispersion characteristics. We classify the SC reports in three types: convex anomalous dispersion (Type I), all-normal dispersion (Type II), and dispersion with multiple ZDWs (Type III). Different dispersion types have different mechanisms, and the detailed analyses of the spectral broadening mechanisms are presented. According to our classifications, the representative works of various materials are displayed. Specifically, our recent work on a $Si_3N_4$ horizontal slot waveguide features Type II dispersion and three-octave coherent SC ranging from 504 to 4229 nm can be obtained. Moreover, the SCG based on the second-order nonlinearity is also introduced briefly and discussed Section 6. Finally, we provide perspectives on the SC spectral coverage, the realization of various dispersion curves, and the novel materials, which are the key aspects of the SCG in nanophotonic waveguides.

## 2. Materials

### 2.1. Basic Characteristics

Since the SCG typically utilizes the nonlinear optical processes, a comprehensive survey on various nonlinear materials is necessary. **Table 1** provides the summary of the common nonlinear waveguide media for SCG. The basic material characteristic parameters of SCG process, involving the semiconductor band gap, the corresponding band gap wavelengths, and the transparent window of these materials are given in the table. Moreover, some media need to consider the TPA and the subsequent free carrier absorption (FCA) and free carrier dispersion (FCD). TPA, FCA, and FCD result in the optical loss, which decreases the peak power and therefore suppresses the spectral broadening in the SCG progress.

As one example, aluminum nitride (AlN) is the noncentrosymmetric media, thus both the quadratic $\chi^{(2)}$ and the cubic $\chi^{(3)}$ nonlinear processes play the role in the nonlinear process. The direct band gap of AlN is >6 eV[139] and AlN has wide transparent window from ultraviolet (UV) (200 nm)[140] to middle infrared (mid-IR) wavelengths (10 μm).[141] The loss of AlN waveguide can achieve as low as 0.6 dB $cm^{-1}$ at telecom wavelengths.[142,170–171] $LiNbO_3$ is also a platform with strong $\chi^{(2)}$ and moderate $\chi^{(3)}$ nonlinearity, together with a transparent window from 350 nm to 4.5 μm.[144] The band gap of $LiNbO_3$ is 4.9 eV.[143] The fabricated $LiNbO_3$ waveguides has a low propagation loss of 0.16 dB $cm^{-1}$ at 1560 nm.[145]

**Table 1.** The basic performance of waveguide platforms for SCG.

| Material | Band gap energy [eV] | Band gap wavelength [μm] | Transparent window [μm] | TPA wavelength [μm] | FCA | Experimental loss [dB cm$^{-1}$] |
|---|---|---|---|---|---|---|
| AlN | 6.1[139] | 0.203 | 0.2[140]–10[141] | 0.406 | × | 0.6[142] |
| $LiNbO_3$ | 4.9[143] | 0.253 | 0.35–4.5[144] | 0.506 | × | 0.16[145] |
| Si (indirect) | 1.12[139] | 1.107 | 1.1[79]–8[146] | 2.214 | √ | 0.1[147] |
| $SiO_2$ | 8.9[148] | 0.1 | 0.2[149]–3.5[150] | 0.279 | × | $7 \times 10^{-4}$[151] |
| $Si_3N_4$ | 5.3[152] | 0.234 | 0.4–4.5[87] | 0.468 | × | 0.001[153] |
| Ge (direct) | 0.82[146] | 1.512 | 1.8[80]–14[146] | 3.024 | √ | 2.5[154] |
| SiGe ($Si_xGe_{1-x}$) | 0.82–1.11[139] | 1.060–1.5 | <8–14[146] | 2.120–3.024 | √ | 1[155] |
| $As_2S_3$ | 2.4[156] | 0.517 | 0.6[149]–12[157] | 1.033 | × | 0.05[102] |
| $As_2Se_3$ | 1.77[139] | 0.701 | 1[149]–15[157] | 1.401 | × | $7.6 \times 10^{-4}$[158] |
| GeAsSe ($Ge_xAs_yGe_{1-x-y}$) | 1.7–1.96[159] | 0.633–0.729 | 0.7–33[160] | 1.265–1.459 | × | 0.5[161] |
| GeSbS ($Ge_xSb_yS_{1-x-y}$) | 1.8–2.3[101] | 0.539–0.775 | >12[101] | 1.078–1.550 | × | 0.56[162] |
| InGaP | 1.9[105] | 0.653 | 0.69–24.8[163] | 1.305 | √ | 12[105] |
| AlGaAs ($Al_xGa_{1-x}As$) | 1.6–1.79[24] | 0.693–0.775 | 0.7–17[149] | 1.385–1.550 | × | 1[164] |
| a-Si:H | 1.7–1.8[139] | 0.689–0.729 | 0.78–4[149] | 1.378–1.459 | × | 2.21[114] |
| $Ta_2O_5$ | 4.2[112] | 0.295 | 0.35–10[165] | 0.590 | × | 2.4[8] |
| $TiO_2$ | 3.2[166] | 0.388 | 8–13[167,168] | 0.775 | × | 2.2[169] |

Si photonics platform is one of the most common and mature integrated optical platforms. The Kerr nonlinear-index coefficient ($n_2$) of Si is 400 times higher than silica. Si optical waveguide has the characteristics of high index contrast and low cost. The energy gap of Si is 1.12 eV[139] and the corresponding wavelength is 1.1 μm. The transparent window of Si is from 1.1 to 8.5 μm,[79,146] and it has a strong absorption band around 9 μm.[146] Meanwhile, Si suffers from the high nonlinear absorption due to the TPA,[121] and thus the optical power is limited significantly in nonlinear applications. The TPA of Si has to be considered in the wavelength range from 1.1 to 2.2 μm, when the launched optical power is high. However, for the wavelength beyond 2.2 μm, the effect of TPA becomes weak enough.[137] The propagation loss of Si is below 0.1 dB cm$^{-1}$ from 2 to 5 μm.[147] Ge is also the group IV element, featuring the direct band gap energy of 0.82 eV[146] and a wider transparent window up to 14 μm.[80,146] The propagation loss is on the level of 2.5 dB cm$^{-1}$ in the mid-IR wavelength range.[154] As alloy materials, the band gap of SiGe is determined by the material composition.[139] The material properties of SiGe can be controlled by balancing the Ge concentration. Its transparent window can usually achieve up to 8 μm, and it is possible to be further extended to 14 μm with lower Si concentration. Propagation losses of SiGe are measured as low as 1 dB cm$^{-1}$ in the mid-infrared (MIR) wavelength range.[155] Group IV photonics materials have the compatibility with the complementary metal oxide semiconductors (CMOS) process. A few other Si-related platforms also offer CMOS compatibility. Moreover, they provide negligible nonlinear loss at telecommunication wavelengths due to their inherent large band gap. The band gap of $SiO_2$ is 8.95 + 0.05 eV,[148] and the absorption loss of $SiO_2$ increases rapidly for wavelength longer than 3.5 μm,[150] and the low loss window is from 0.2[149] to 3.5 μm. The loss of silica waveguide is measured to be 0.07 dB m$^{-1}$[151] in the telecommunications window by using backscatter reflectometry. Finally, the energy band gap of $Si_3N_4$ is large and has a negligible TPA coefficient.[87,152] $Si_3N_4$ features a wide transparent window from the visible (0.4 μm) to the mid-IR (4.5 μm) range,[39,87] and the loss of $Si_3N_4$ waveguides can be as low as 0.1 dB m$^{-1}$ at 1550 nm.[153]

Table 1 also lists the alloy of complex composition, such as the III–V materials and the chalcogenide glasses. These materials provide more flexibility in terms of adjusting the concentration ratio of the components. The band gap can also be engineered by changing the concentration ratio of the material to avoid the TPA in some particular wavelengths. III-V materials offer the possibility to overcome the TPA of Si and they also have large third order nonlinearities. For example, InGaP or $A_{l_x}Ga_{1-x}As$ (both grown on a GaAs substrate) have the efficient nonlinear optical processes in the telecommunication wavelength range. When InGaP lattice matched to GaAs, the corresponding band gap is 1.9 eV,[105] which is larger than the TPA energy at 1550 nm. This is also an alternative platform for on-chip nonlinear applications at communication bands.[172] The reported loss of InGaP waveguide is 12 dB cm$^{-1}$ at 1540 nm, which is relatively high.[105] Conventional $Al_xGa_{1-x}As$ waveguides are also grown on the GaAs substrate. The band gap of $Al_xGa_{1-x}As$ is from 1.60 to 1.79 eV,[24] and it can be adjusted by controlling the composition of the aluminum. The propagation loss of the fabricated AlGaAs-on-insulator (AlGaAsOI) waveguides is as low as 1 dB cm$^{-1}$ at telecom wavelengths.[164]

Chalcogenide glasses contain the chalcogenide elements, sulphide, selenides or tellurides, which are usually the dominant constituent, combined with some other materials such as Ge, arsenic (As), phosphorus (P), antimony (Sb) or Si. Chalcogenide glasses have wide transparent spectral range. The transparent windows for Sulfur (S), selenium (Se), and tellurium (Te) are up to about 12 μm, up to around 16 μm, and beyond 20 μm,[173] respectively. Specifically, the transparent window of $As_2S_3$ is 0.6[149]–12 μm,[157] while it is 1[149]–15 μm[157] for $As_2Se_3$. The band gap energy and loss also impact the SCG process in these nonlinear chalcogenide glasses. The band gap of $As_2S_3$ is 2.4 eV,[139,156] and $As_2Se_3$ has a smaller band gap of 1.77 eV.[139] The optical loss of $As_2S_3$ chalcogenide waveguides is as low as

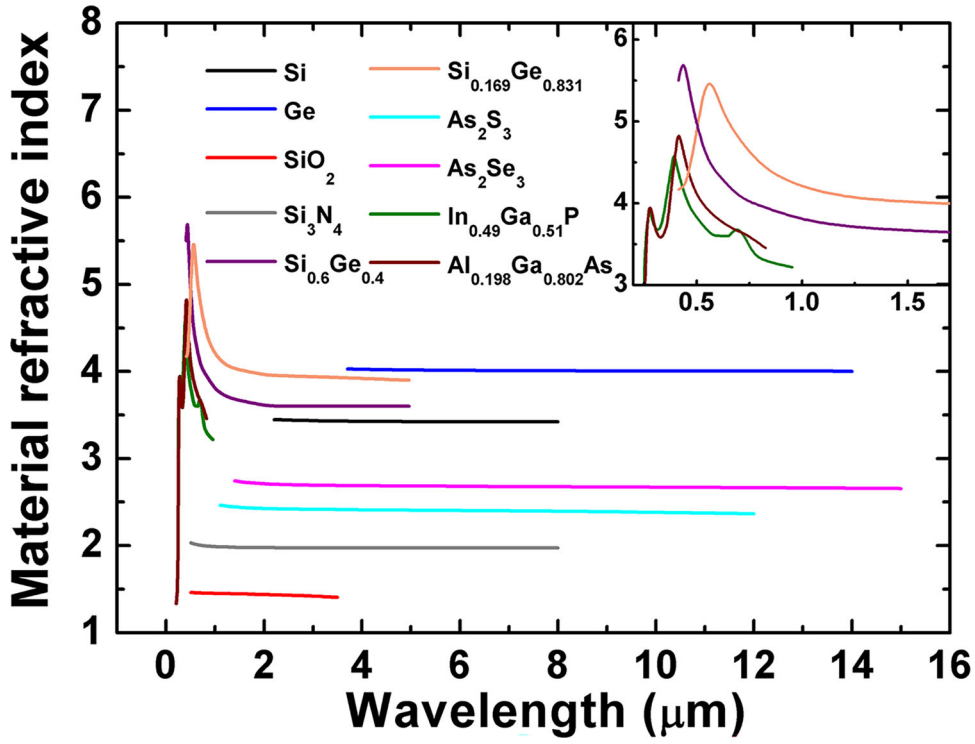


**Figure 1.** Refractive index of the materials used for SCG in the nanophotonic waveguides.

0.05 dB $cm^{-1}$ at 1550 nm.[102] The optical losses of the best reported sample for $As_2Se_3$ chalcogenide glass is $7.6 \times 10^{-5}$ dB $mm^{-1}$ from 1 to 10 μm,[158] which is the lowest loss among the summarized waveguides over different material platforms. For the Ge glass, the band gap of GeAsSe depends on the concentration of Ge, and the value increases from 1.7 to 1.96 eV with the content of Ge.[159] The band gap energy of GeSbS glasses also corresponds to the percentage of different materials, which is from 1.8 to 2.3 eV.[101] Specifically, $Ge_{23}Sb_7S_{70}$ is the representative concentration and its band gap is 2.3 eV.[174] The complete transparent window of GeAsSe glass is spanning from 0.7 to 33 μm,[160] and the window of GeSbS is beyond 12 μm.[101] Moreover, the measured loss of GeAsSe glass is 0.5 dB $cm^{-1}$ in SCG applications between 3 and 7 μm.[161] GeSbS waveguide with low propagation loss has been fabricated, and the corresponding loss is reduced to 0.56 dB $cm^{-1}$ at 1550 nm.[162]

The summary also includes some seldom used materials in the SCG researches. A-Si:H has a higher band gap,[139] thus its transparent window at short wavelength regime is wider than that of Si. Its loss is 2.21 dB $cm^{-1}$, which is measured by the cutback method at 1950 nm.[114] Tantalum pentoxide ($Ta_2O_5$) is also the CMOS-compatible material. Its band gap is 4.2 eV and it has small extinction and thermal-optical coefficients.[112] The transparent window of $Ta_2O_5$ spans from 0.35 to 10 μm,[165] and the propagation loss of the $Ta_2O_5$ channel waveguide is 2.4 dB $cm^{-1}$ at 800 nm.[8] Moreover, Titanium dioxide ($TiO_2$) has attracted lots of interest recently. The transparent window of $TiO_2$ covers from 8 to 13 μm,[167,168] and its band gap is relatively high at 3.2 eV.[166] The propagation losses of $TiO_2$ strip waveguides could achieve 2.2 dB $cm^{-1}$ at 1.55 μm.[169]

### 2.2. Material Dispersion

The bandwidth of broadened spectrum is mainly determined by the interaction between CD and nonlinearity. The overall CD includes material dispersion and waveguide dispersion. The waveguide dispersion depends on the geometric parameters of the waveguiding structure, while the material dispersion is mainly affected by the refractive index of the material. **Figure 1** shows the refractive index of commonly used waveguide materials. Si, as the most mature platform, has high index contrast with good light confinement, and also supports various novel structures. The material refractive index of Si is given by ref. [175]. Compared with Si, the material refractive index of silica is relatively low,[176] which is unfavorable for tight mode confinement at small footprint. $SiO_2$ is always used as the cladding material for integrated waveguides.[89, 177–180] Recently, some reports introduced high-index doped silica waveguide for higher refractive index.[181] The material refractive index of $Si_3N_4$ (about 1.98)[182] is higher than that of silica. $Si_3N_4$ is also an attractive material of non-silicon platform for dispersion engineering. Although as a relatively new CMOS platform, various structures of $Si_3N_4$ waveguides have already been reported in refs. [87, 183–186]. Ge[187] exhibits higher material refractive index than Si, and thus the refractive index of the SiGe alloy is also higher than the one of Si. The measured refractive index of SiGe is determined by the atomic fraction of Ge. The material refractive index increases when the alloy composition is heavily doped Ge. We enumerate two types of mole fraction for SiGe alloy. $As_2S_3$ and $As_2Se_3$ are the chalcogenide glasses with relatively simple composition. Their material refractive indices are larger than $Si_3N_4$,[79,188] which facilitates the stronger

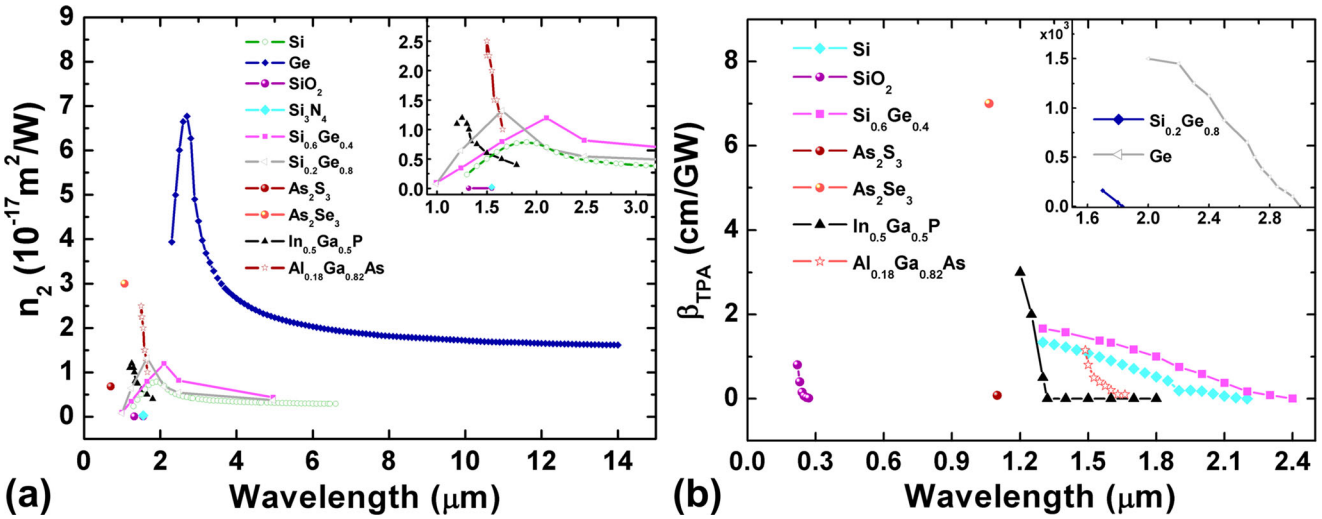


**Figure 2.** a) Nonlinear-index coefficient of the materials considered for SCG. b) TPA coefficient $\beta_{TPA}$ of the materials considered for SCG.

mode confinement. The material refractive indices of III–V materials are also shown in Figure 1. $Al_xGa_{1-x}As$ with $x = 0.198$ for Al[189] and $In_xGa_{1-x}P$ with $x \approx 0.5$ for In[190] matched to GaAs are the typical concentrations. The information given in Figure 1 can properly provide the basis for choosing waveguide core and cladding materials.

### 2.3. Nonlinearity Characteristics

The second-order nonlinearity effects are governed by the second-order susceptibility $\chi^{(2)}$, including SHG and sum frequency generation (SFG). Specially, $\chi^{(2)}$ is zero for the media with inversion symmetry. $SiO_2$ is the symmetric molecule, which normally lacks the second-order nonlinearity effects.[42] Meanwhile, the THG and the FWM originate from third-order susceptibility $\chi^{(3)}$, and most of the SCG processes are formed by the intrinsic $\chi^{(3)}$ susceptibilities of meida. In addition to the dispersion effect, high nonlinearity is required for the effective SCG at low peak power of the input pulse. The nonlinear phenomenon is associated with the nonlinear part of the refractive index, that is, the wavelength-dependent $n_2$. **Figure 2**a depicts the $n_2$ of the common waveguide media. If the conventional fiber material (e.g., $SiO_2$) is considered as a baseline for comparison with the other materials, the measured $n_2$ of Si is about two orders of magnitude higher than that of $SiO_2$[121] and $Si_3N_4$ also offers one order of magnitude higher $n_2$ than the one of $SiO_2$.[94] Ge has much larger $n_2$ (about 2800 times) than $SiO_2$.[191] The $n_2$ of SiGe alloy is between the ones of its composited materials Si and Ge. The slightly doped $Si_{0.6}Ge_{0.4}$ and the heavily doped $Si_{0.2}Ge_{0.8}$ are two types of representative concentrations.[191] Based on ref. [191], Si and lightly doped SiGe alloy are treated with the indirect model, while Ge and heavily doped SiGe alloy can be applied with the direct model. Chalcogenide glass has high linear and nonlinear refractive indices, which allows stronger nonlinear interaction within short propagation distance. The strong $n_2$ of $As_2S_3$ glass is about 2 orders of magnitude larger than the one of $SiO_2$.[192] $As_2Se_3$ glass possesses high third-order Kerr nonlinearity, and the order of magnitude is close to Ge (about 1200 times higher than $SiO_2$).[193] For III–V material systems, the theoretical nonlinear-index coefficient of $In_xGa_{1-x}P$ ($x \approx 0.5$) is two orders of magnitude higher than the one of $SiO_2$.[194] The measured value of $Al_xGa_{1-x}As$ with the Al concentration of $x = 0.18$ is about three orders of magnitude higher than that of $SiO_2$.[195] Higher nonlinearity makes these waveguides as good candidates for effective SCG with shorter waveguide length.

The nonlinear loss due to TPA, has impeded the potential application of some nonlinear platforms in the telecom window. TPA means the energy vanishes within the wavelength range that the energy of two photons is enough for energy level transition. TPA decreases the optical power nonlinearly, further weakens the spectral broadening associated with SCG, and clamps the bandwidth. TPA acts as the significant factor to impact the SCG for the media with large TPA coefficient when the optical intensity is strong. For example, Si,[79] Ge, and SiGe alloy[191] of different concentration are the typical materials that possess TPA in the telecommunication bands. The TPA coefficient $\beta_{TPA}$ as a function of wavelength is showed in Figure 2b. III–V materials[194,195] and the chalcogenide glasses[192,196] are also included in Figure 2b. The $\beta_{TPA}$ of Ge is the largest among the mentioned material and the measured value can achieve close to 1500 cm $GW^{-1}$, which is almost three orders of magnitude higher than that of Si. The maximum $\beta_{TPA}$ of Si is >1.3 cm $GW^{-1}$. The TPA coefficient of $As_2Se_3$ is 7 cm $GW^{-1}$ at 1.064 μm, and the corresponding value of $As_2S_3$ is 0.08 cm $GW^{-1}$ at 1.064 μm. The experimental data of $Al_{0.18}Ga_{0.82}As$ is 1.15 cm $GW^{-1}$ at 1.4875 μm. and the $\beta_{TPA}$ of $In_{0.5}Ga_{0.5}P$ is 3 cm $GW^{-1}$ at 1.2 μm. For $SiO_2$, the measured TPA coefficients are all concentrated at short wavelengths[197] and the maximum values is 0.8 cm $GW^{-1}$ at 220 nm. Additionally, there is no nonlinear absorption that has been observed in the $Si_3N_4$ waveguides, and thus its TPA coefficient is negligible.[87] The low nonlinear losses are critical in integrated platforms for nonlinear applications, which is beneficial to attain the smaller footprint and lower energy consumption.

## 3. Fundamental Equations

### 3.1. Nonlinear Propagation Equation

The generalized nonlinear Schrodinger equation (GNLSE) is used to describe the evolution of pulse propagation in simulations,[42] which is expressed as:

$$\frac{\partial A}{\partial z}+\frac{1}{2}\left(\alpha\left(\omega_0\right)+i\alpha_1\frac{\partial}{\partial t}\right)A-i\sum_{n=1}^{\infty}\frac{i^n\beta_n}{n!}\frac{\partial^n A}{\partial t^n}$$
$$=i\left(\gamma\left(\omega_0\right)+i\gamma_1\frac{\partial}{\partial t}\right)\left(A\left(z,t\right)\int_0^{\infty}R\left(t'\right)\left|A\left(z,t-t'\right)\right|^2dt'\right) \quad (1)$$

where $A$ is the electric field envelope. The frequency dependence of Kerr nonlinear coefficient $\gamma$ and the optical loss $\alpha$ needs to be considered for SCG, that is,

$$\gamma(\omega)=\gamma(\omega_0)+\gamma_1(\omega-\omega_0) \quad (2)$$

$$\alpha(\omega)=\alpha(\omega_0)+\alpha_1(\omega-\omega_0) \quad (3)$$

The first order derivative over frequency $\gamma_1 = d\gamma/d\omega$ term makes the group velocity dependent on the optical intensity, which results in the self-steepening phenomenon, $\omega_0$ is the carrier frequency. Commonly, one can calculate the nonlinear coefficient $\gamma$ with the nonlinear Kerr index $n_2$ (units of $m^2\ W^{-1}$), $\gamma(\omega_0) = \omega_0 n_2/cA_{\text{eff}}$, and $A_{\text{eff}}$ represents the effective mode area of the waveguide. The $n_2$ of various waveguide core materials can be obtained through Figure 2a. Specifically, when the waveguides are with inhomogeneous transverse structure, such as the slot waveguide, the generalized full vectorial model of the nonlinear coefficient $\gamma$ and effective mode area $A_{\text{eff}}$ should be used in the equations,[184] which considers the modal distribution into different materials. The $n_2$ is replaced by $\bar{n}_2$, and $\bar{n}_2$ represents the weighted average nonlinear-index coefficient according to the field distribution over an inhomogeneous cross-section. The multi-order summation term of $\beta$ represents the effects of CD, and $\beta_n$ is the $n$-th order Taylor series expansion of the mode-propagation constant. The second-order dispersion parameter $\beta_2$ is usually used to describe the dispersion of the group velocity, which is responsible for pulse broadening. When the pulse width of the input pulse is shorter than 5 ps, that is, the fs pulse we focus in Section 5.2, higher-order nonlinear and dispersive effects should be considered in the GNLSE. The third-order dispersion (TOD), self-steepening, and intrapulse Raman scattering should be taken into consideration. To model the nonlinear process over ultra-broad band, such as SCG, more higher-order or even all-order dispersion terms need to be included. The integral of $R(t)$ represents the energy transfer resulting from intrapulse Raman scattering, and $R(t)$ is the Raman response function,[42] which is usually expressed as:

$$R\ (t)=\left(1-f_{\text{R}}\right)\ \delta\left(t\right)+f_{\text{R}}\frac{\tau_1^2+\tau_2^2}{\tau_1\tau_2^2}\exp\left(-\frac{t}{\tau_2}\right)\sin(\frac{t}{\tau_1}) \quad (4)$$

$\delta(t)$ is the instantaneous electronic contribution, where $f_{\text{R}}$ represents the contribution of the delayed Raman response. In practice, $\tau_1$ and $\tau_2$ are the parameters to fit the actual Raman gain spectrum.

Depending on the input pulse width $T_0$ and its peak power $P_0$, the dispersion length $L_{\text{D}}$ and the nonlinear length $L_{\text{NL}}$ could be obtained:

$$L_{\text{D}}=\frac{T_0^2}{\left|\beta_2\right|} \quad (5)$$

$$L_{\text{NL}}=\frac{1}{\gamma P_0} \quad (6)$$

According to the relative magnitudes of the propagation length $L$, $L_{\text{D}}$, and $L_{\text{NL}}$, the propagation behavior can be classified into four categories. When the propagation length $L$ is close to both $L_{\text{D}}$ and $L_{\text{NL}}$, dispersion and nonlinearity act together along the pulse propagation, and this is the most common condition. Based on the aforementioned case, split step Fourier method is usually used to solve the nonlinear equation. The core technique of this method is to divide the propagation length into many small segments, and then to assume that the dispersion and nonlinear effects act independently in each segment. For example, only the nonlinearity acts in the odd steps, while merely the dispersion exists in the even steps.

### 3.2. Coherence Equation

The coherence of the SC can be calculated by the modulus of the complex degree of first-order coherence:[42]

$$g_{12}\ (\omega)=\frac{\langle\widetilde{A_1}^{*}\left(L,\omega\right)\widetilde{A_2}\left(L,\omega\right)\rangle}{\left[\langle\left|\widetilde{A_1}\left(L,\omega\right)\right|^2\rangle\langle\left|\widetilde{A_2}\left(L,\omega\right)\right|^2\rangle\right]^{\frac{1}{2}}} \quad (7)$$

where $\tilde{A}_1$ and $\tilde{A}_2$ are the Fourier transforms of two neighboring pulses, and the angular brackets represent an ensemble average over independently generated pairs of the SC spectra. Moreover, the formula is a function of frequency. The coherence is numerically calculated by adding random noise to the input pulse.[198] Quantum noise model (one photon per mode noise model)[62,67,199] can be chosen and solved repeatedly in the simulations. The experimental measurements of the coherence can be obtained by observing the interference fringes generated through two successive pulses.[200–203]

## 4. Waveguide Structure and Properties

### 4.1. Various Types of Uniform Waveguides for Supercontinuum Generation

**Figure 3** illustrates the cross section of different integrated waveguides for SCG. First, one can see that how to choose different material combinations of the core, substrate, and cladding for the appropriate index contrast. The SOI waveguide is widely used due to its tight light confinement, low cost, and CMOS technology compatibility. The material absorption from the oxide cladding and substrate causes these extra losses when the

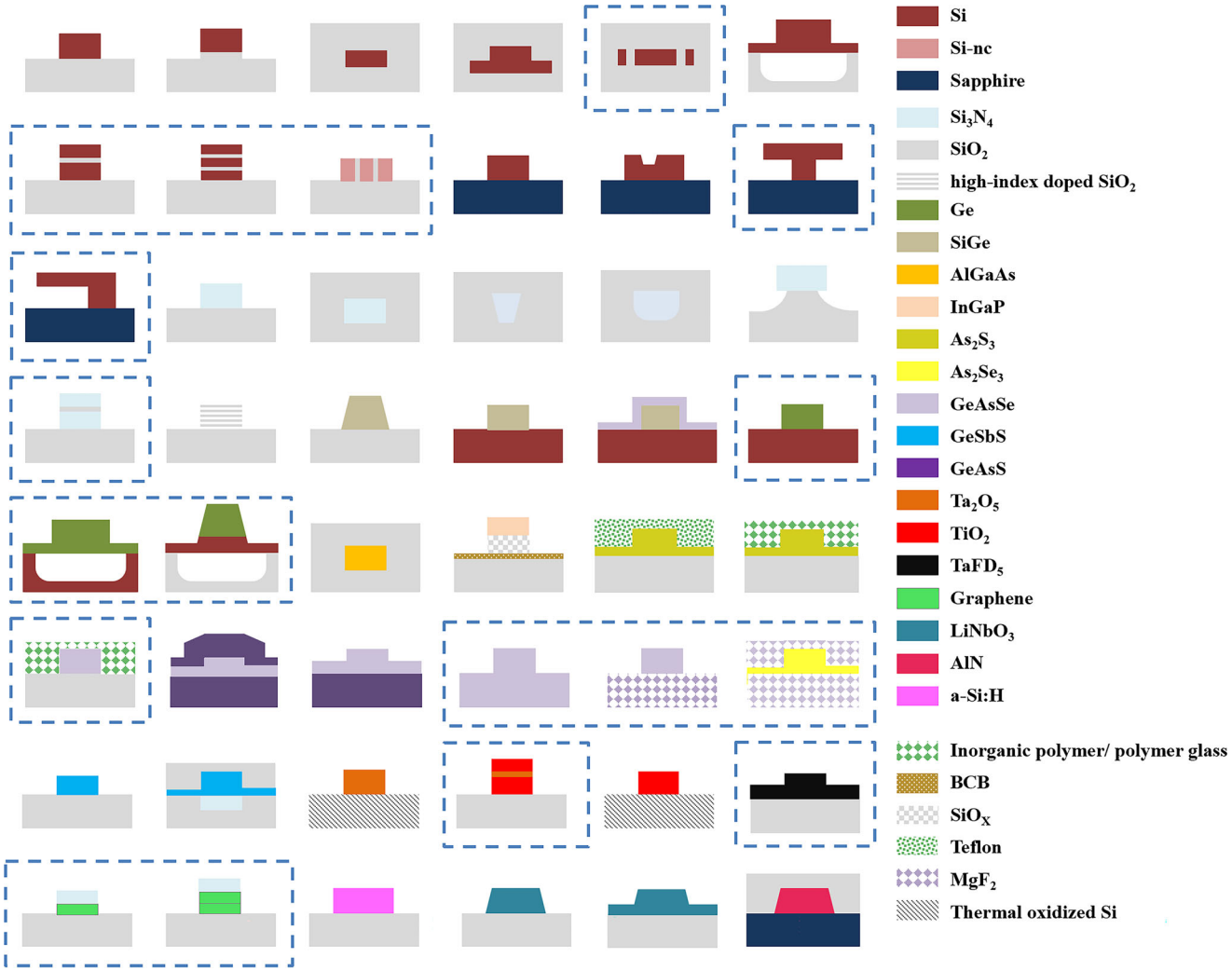


**Figure 3.** Cross sections of different integrated waveguide types for SCG.

operating wavelength is beyond the transparent window for the cladding and substrate materials. For example, the $SiO_2$ cladding or substrate could result in large energy consumption as the wavelength is beyond 3.5 μm.[204–206] However, The air-cladded Si waveguide can avoid extra losses due to the limited transparent window of the external cladding materials.[125,207] The transparency of sapphire substrate is up to 5 μm, which could be used to further extend the low-loss operating window.[208–211] For silica waveguide, in addition to considering the transparent window, how to achieve enough index contrast between the waveguiding core and the substrate is the main issue. The high-index doped silica glass is the typical solution to provide the high index contrast (compared to silica fibers).[181] $Si_xGe_{1-x}$ waveguide could be obtained by growing Ge on the SOI layer with different Ge mass flow during the growth process. SiGe waveguides on a Si substrate with air or chalcogenide cladding were also demonstrated.[84,212–214] SCG in the SiGe waveguide is still limited at wavelengths larger than 8.5 μm owing to the presence of Si, thus germanium-on-silicon platform has been investigated for SCG. Moreover, the III–V materials have been proven to be an attractive nonlinear material platform for SCG. Many III–V material compositions such as InGaP and $Al_xGa_{1-x}As$ are usually grown on a GaAs substrate. However, in order to achieve high index contrast, which is similar to the requirement in the SOI platform, removing the GaAs substrate for the growth of the InGaP layer is the commonly used processing method.[105,164] Meanwhile, the relatively high index contrast may produce large scattering loss due to the roughness at the material interface.[215]

Second, we summarize various waveguide shapes including both the theoretical and experimental structures, and introduce various fabrication methods of these structures. Different structures have been applied in the SCG, such as, the wire waveguide,[101,111,112,114,125,181,212,216–221] buried waveguide,[39,222–225] rib waveguide,[173,162,226–232] suspended waveguide,[232,233] waveguide being over-etched into the buried oxide,[206] waveguide with buried silicon oxide layer being under-etched,[234] waveguide with a round-shaped core at the bottom side,[235,236] and the waveguide with sidewall angle.[214,223,237,238] The dotted box in Figure 3 denotes the waveguide structures used for the SCG modelling only, and the remaining ones are

the fabricated structures that have been used in the SCG experiments. The suspended waveguide design can solve the oxide absorption in the traditional SOI structure. The device layer can be grown and written with the pattern by e-beam lithography and reactive ion etching. After that, the substrate was dipped in the solution to remove the oxide layer below the waveguide. Some waveguides have double inverse taper mode converters at both ends with improved coupling efficiency.[222,224,239] The SC generated by the side-slotted waveguide,[225] the horizontal single-slot,[128,240,241] double-slot waveguide,[242] vertical slot waveguide,[127] the upright T and inverted L waveguide,[126] and chalcogenide glasses with special substrate or cladding remains in the stage of numerical simulation. Furthermore, similar slot structure can be fabricated in previous reports for low-loss investigation,[243] which is based on low-pressure chemical vapor deposition, plasma enhances chemical vapor deposition, dry etch, and other fabrication steps.

### 4.2. Dispersion Engineering

The overall CD of the guided mode contains the material dispersion mentioned above and the waveguide dispersion. It can be calculated by a full vector mode solver, considering the wavelength-dependent material refractive index $n(\lambda)$. The dispersion parameter ($D$) can be expressed as the following:[42]

$$D = -\frac{\lambda}{c}\left(\frac{d^2 \mathrm{real}\left(n_{\mathrm{eff}}\right)}{d\lambda^2}\right) \tag{8}$$

where $\lambda$ is the wavelength, and $c$ is the speed of light in vacuum. The mode-propagation constant $\beta$ can be obtained through the relations of effective index and wavelength:[42]

$$\beta = n_{\mathrm{eff}}\ (\omega)\,\frac{\omega}{c} \tag{9}$$

Also, $\beta$ can be expended as a Taylor series about the center frequency $\omega_0$:[42]

$$\beta\ (\omega) = \beta_0 + \beta_1\left(\omega - \omega_0\right) + \frac{1}{2}\beta_2\left(\omega - \omega_0\right)^2 + \cdots \tag{10}$$

where $\beta_2$ represents the group velocity dispersion (GVD) and is responsible for the pulse broadening. Higher-order or all-order dispersion terms are always included in the GNLSE. The CD can be tailored for various applications. One can tune the waveguide dimensions when the material combinations are determined. Some novel structures can greatly enhance the mode confinement and the capability of dispersion engineering. Strip waveguide is the simplest structure, of which only the waveguide height and width are variable. Its corresponding dispersion profile is convex, and the position and number of ZDW can be tailored by changing the waveguide dimension. On the basis of strip waveguide, the rib waveguide provides more adjustable structural parameters to tailor the CD.[173,162,226–231] Rib waveguide usually has larger mode field distribution, and it is easier to leak into the substrate in the long wavelength range. Furthermore, adding the overlayer of the strip or rib waveguide makes the index contrast relatively small between the core and cladding. The relatively low index contrast may suppress the strong and fast-changing waveguide dispersion, which could increase the dispersion flatness. Through these methods, the tip of the convex dispersion profile could be relatively flattened within the limited range. Further flattening the dispersion in a broader wavelength range needs to introduce additional waveguide dispersion to balance the convex profile. A low index layer can be sandwiched between two high-index layers, that is, which forms a slot waveguide. Due to the abrupt refractive index between two media, the electric field has the discontinuity at the high-refractive-index-contrast interfaces and the mode with a polarization normal to the interfaces is significantly enhanced within the slot region. A large fraction of the light can be confined in the slot layer, and this enables a dramatic field enhancement in the slot to control the nonlinearity. Furthermore, the slot layer provides more freedom to tailor the CD. Slot waveguides have been utilized to tailor the dispersion over broadband more precisely, and more ZDWs can be achieved in the dispersion profile. At short wavelength, the low-index slot layer serves as a barrier to confine most of the field within the upper/lower high-index region, and the mode shape is similar to a strip mode. As the wavelength increases, the overall modal field moves downward/upward and the light is enhanced by the slot layer to form a slot mode.

The coupled-mode theory could be used to explain the mechanism of flattened dispersion engineering. When the effective indices of the two modes are close to each other, an anti-crossing effect occurs due to the relatively strong mode coupling between the strip mode and slot mode, which would form the symmetric and anti-symmetric modes.[244,245] From the symmetric mode, at the crossing wavelength, the additional strong negative concave dispersion is formed, which could be used to compensate for the existent convex dispersion profile. As a result, the overall CD can be flattened over broadband range. Based on this mechanism, the dispersion curve with three or four ZDWs can be formed.[126–128,136,137,246,247] The characteristic of dispersion profile is no longer convex but saddle-shaped. The flattened dispersion with four ZDWs could also be formed by the bilayer structure in ref. [135]. A new type of waveguide with 5 or even 6 ZDWs is also proposed recently by combining these two structures.[248] The mode experiences two transitions across different layers. The first process is the mode transition from the strip mode to the slot mode in the inner trilayer waveguide. The inner part together with the coating can be seen as the waveguide core, and the mode shifts from the upper core toward the slab part, which performs as the bilayer waveguide.[135] These two transitions form two saddles in the dispersion profile and it features the most ZDWs ever reported.

### 4.3. Multi-Stage Waveguides for Supercontinuum Generation

Generally, the effective refractive index profile of the guided mode is determined by the material platform and waveguiding structure (**Figure 4**). However, only adjusting the cross section of the waveguide would limit the flexibility on effective refractive index tailoring. Some studies reported SCG in cascaded waveguides or waveguides with variable cross sections.[140,249–253] The varying geometry of a waveguide could provide more possibilities to tailor the SC properties. For instance, varying the shape

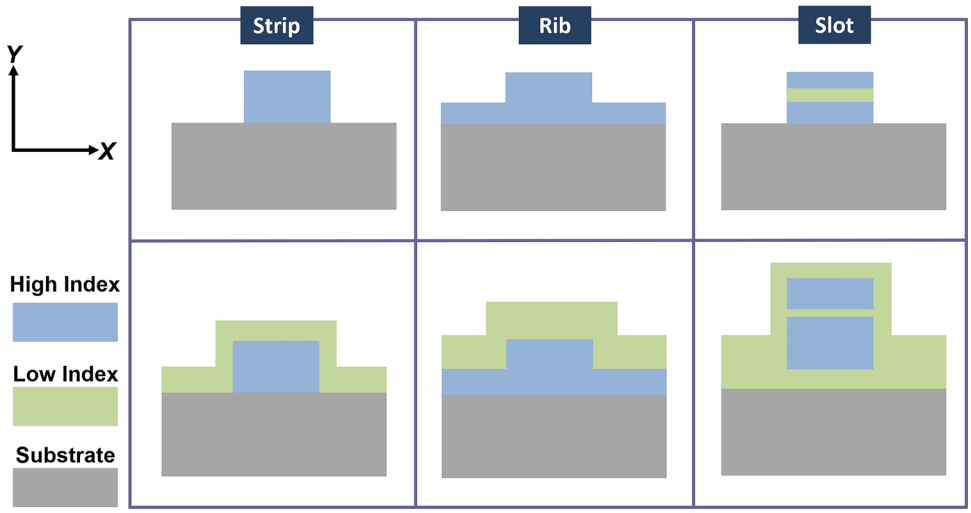


**Figure 4.** Schematic diagram of different waveguide structures for the dispersion engineering.

of a waveguide along the propagation direction is utilized to do the dispersion management, and then enhance the SC and its coherence.[249,251,252] Periodic structures are widely used to support the quasi-phase-matching (QPM) condition. Such as periodically poled lithium niobate (PPLN),[254] the SHG induced by $\chi^{(2)}$ nonlinearities could broaden the SC bandwidth. In addition, the phase matching condition between soliton and dispersive wave (DW) could be satisfied through periodic modulations of material nonlinearity.[255] For instance, Bragg grating could realize the signal enhancement at certain wavelengths where DWs are weak, or provide larger anomalous dispersion.[253] Therefore, the multi-stage waveguides provide more freedom of dispersion engineering and nonlinear effects, even though the fabrication process of these structures is relatively complicated.

## 5. Supercontinuum Generation Based on Third-Order Nonlinearity

The majority of the SCG still relies on the $\chi^{(3)}$ process. In this section, we present the results to illustrate the SCG process based on third-order nonlinearity $\chi^{(3)}$. We first discuss the SC dynamics for long pulses, that is, picosecond even the CW in Section 5.1. The mechanisms and the recent works of SCG depend on femtosecond pulse are discussed in Section 5.2. The SCG using the femtosecond pulse is the scenario we focus on.

### 5.1. Pump in the Picosecond to the Continuous-Wave Regime

The mechanisms of broadband SCG using longer pulses, that is, the picosecond, nanosecond, and even the CW are relatively different from the femtosecond dynamics mentioned above. The FWM, modulation instability (MI), SPM, and Raman scattering are often the dominant mechanism when pumping in anomalous dispersion.[62,204,256,257] The soliton order $N$ determines the competition of fission against MI. There are the generally accepted conditions. When $N < 15$, the dominant mechanism tends to be the soliton fission. However, if $N >> 15$, MI dominates in the SCG.[42,258–260] MI results in the breakup of the long pulse radiation into a series of ultrashort pulses. No matter which process mentioned above requires anomalous dispersion. The spectrum generated by MI usually has the broad sidebands and the narrowband peaks.[114,204,228,261] All of the generated peaks satisfy the phase matching condition,[204] and the MI can be interpreted as a FWM process that is phase-matched by the SPM. Even if the MI is the main mechanism for SCG, DWs can also be generated.[262,263] Furthermore, the SRS can generate new frequency components, but the spectrum broadening is asymmetric due to the Stokes band on the long-wavelength side. If the input peak power is larger than the Raman threshold, the SRS results in the red-shifted spectrum.[42]

### 5.2. Pump in the Femtosecond Regime

**Figure 5** represents the graphical summary of the most relevant experimental results on SCG in waveguides with commonly used materials. Vertical color shading represents various types of the laser source and the position of multi-colored dots mark pump wavelengths: optical parametric amplifier (OPA), optical parametric oscillator (OPO), and others (through a high nonlinear fiber, etc.). The lines with different colors denote the core material of the waveguide, and the SC with −30 dB spectral bandwidth is represented by the spanning range of the lines. The experimental details are provided below. The solid lines show the experimental SC generation results based on common convex anomalous dispersion (Type I), and the dashed lines indicate the SC results based on all-normal dispersion (Type II). The finer lines express the further spectral broadening in the following reports by the same team.

In Figure 5, we can see that Si and $Si_3N_4$ are the commonly used waveguide materials for SCG experimental reports. The broadest spectrum generated in the SOI platform was from a suspended waveguide,[233] and a continuous broad spectrum of 1.32 octave (2–5 μm) was observed with a pump pulse wavelength of 4 μm. The silicon-on-sapphire (SOS) platform is a more suitable for MIR SC generation beyond 4 μm. A SOS nanowire was re-

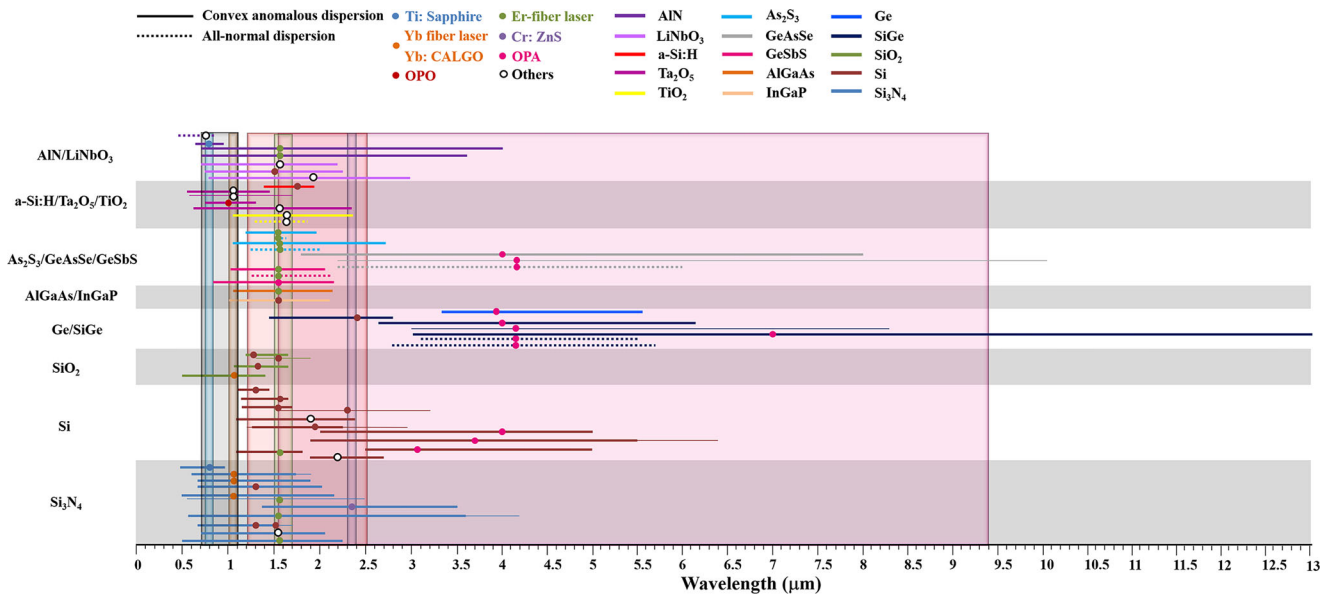


**Figure 5.** Overview of the experimental results on SCG using the most prevalent waveguide materials.

ported by N. Singh et al., which could cover a spectral range from 1.9 to beyond 5.5 μm by pumping at 3.7 μm.[207] For $Si_3N_4$ waveguide, the widest experimental results of spectra were pumped by an erbium-fiber based femtosecond laser at 1.55 μm in the telecommunication band.[39,264] The SC spanned from 0.56 to 3.6 μm through mid-IR DWs generation of the TE mode. The bandwidth can be further broadened to 4.2 μm by using the thicker waveguides for the TM mode. The covering range of SC generated by $SiO_2$ waveguide was less than 1 μm, due to the relatively low Kerr nonlinearity of $SiO_2$ and the weak confinement. Based on Section 2.3, the Kerr nonlinearity of Ge is higher compared with the one of Si. In a low-loss Ge-on-Si waveguide,[265] a broadband SC covering from 3.33 to 5.55 μm was experimentally generated. Thus compositing Ge to Si also can enhance the optical nonlinearity, the $Si_{0.6}Ge_{0.4}$ on Si waveguides with a top air-cladding had the anomalous dispersion profile, and the SC spanned from 2.63 to 6.18 μm with a bandwidth of 3.55 μm.[212] After the deposition of chalcogenide cladding, the all-normal dispersion was obtained with the SC covering from 3.1 to 5.5 μm.[213] The SC results can also be broadened by larger $Si_{0.6}Ge_{0.4}$ waveguides with air-cladding, which has all-normal dispersion. The SC can be expanded from 2.8 to 5.7 μm.[212] The broadest SC in SiGe alloy was ranging from 3 to 13 μm, which was based on $Si_{0.2}Ge_{0.8}$ waveguide.[266]

The waveguide based on III–V materials, such as AlGaAsOI waveguide and InGaP membrane waveguides, have the high-index-contrast and high effective Kerr nonlinearity. These integrated photonic platforms have not been widely used for SCG, moreover, the bandwidth of the existing SC results was just over 1 μm.[172,267]

Chalcogenide waveguides can produce the broader SC range among the materials mentioned, which could be over 10 μm due to the strong third-order nonlinearity, low nonlinear absorption, and good transparency in the MIR. The generation of a broadband SC spanning from 1.8 μm to beyond 7.5 μm was reported in 2014.[173] It was based on a low-loss rib chalcogenide glass waveguide with a $Ge_{11.5}As_{24}Se_{64.5}$ (GeAsSe) core and a $Ge_{11.5}As_{24}S_{64.5}$ (GeAsS) lower cladding, and the pump was in the anomalous dispersion regime. In 2016, the demonstrated spectrum was extended beyond 10 μm covering from 2.2 to 10.2 μm at a dynamic range of −30 dB by using the same structure.[229] The input pulse was centered at 4.184 μm. The spectrum was also measured by pumping the TE mode in the all-normal dispersion, and a narrower spectrum spanning from 2.4 to 6.5 μm was obtained with significant spectral intensity fluctuation.

Recently, CMOS-compatible materials, such as a-Si:H waveguides, $Ta_2O_5$, and $TiO_2$ platforms have been utilized in SCG.[111,112,114,268,269] The broadest SC was generated in a $Ta_2O_5$ waveguide with $SiO_2$ cladding covering 1740 nm.[269] Nevertheless, the bandwidth is not prominent compared with the others.

$LiNbO_3$ and AlN have also opened alternative possibilities for broadband light sources, due to their strong $\chi^{(2)}$ and $\chi^{(3)}$ nonlinearity simultaneously.[140,145,237,238,256] For AlN photonic-chip waveguides, the SCG from the visible region (0.7 μm) to the MIR (4 μm) relied on short wavelength dispersive wave (SWDW) and long wavelength dispersive wave (LWDW) generation. Among these media, $\chi^{(2)}$ processes attract more attention.[239] Utilizing PPLN is also an effective approach to obtain a broadband SC. The SC started from phase mismatched SHG, and further enhanced by $\chi^{(3)}$ nonlinearities. The bandwidth of SC is 2.2 μm.[254]

In the next part, we survey the preferable experimental results based on waveguides with different materials for SCG, and we classify the researches by their mechanisms between dispersion and nonlinearity. As shown in **Figure 6**, there are three main types to distinguish and summarize for SCG. First, Type I is the convex anomalous dispersion case. When pumping in the anomalous GVD regime, the spectral broadening effects are dominated by soliton-related dynamics. Meanwhile, the profile of dispersion curve is convex without complicated engineering. Next, Type II is the all-normal dispersion case. Soliton fission and DW generation do not occur, and the spectrum broadening is mainly due to the SPM, optical wave-breaking (OWB), and

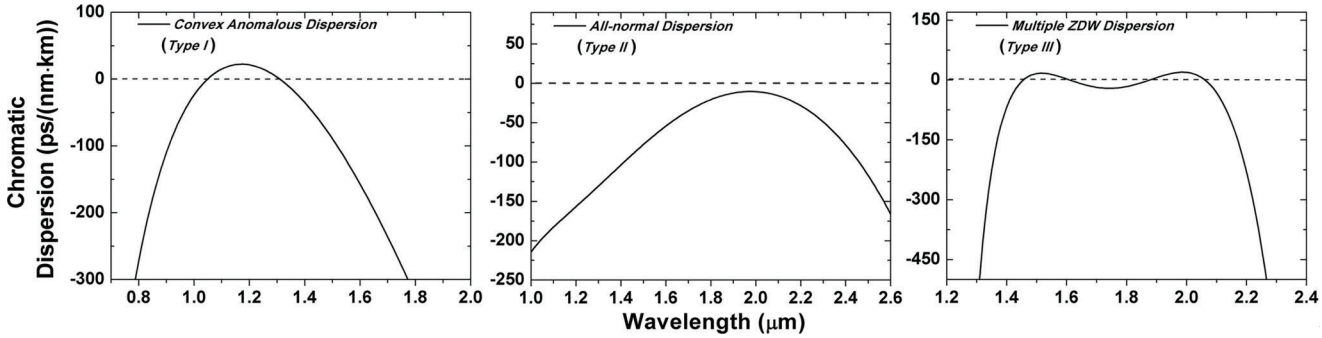


**Figure 6.** Three typical types of dispersion curves used in the SCG processes.

self-steepening. Finally, Type III is the case for the dispersion curve with multiple ZDWs.

#### 5.2.1. Convex Anomalous Dispersion (Type I)

We first simulate the convex dispersion curve based on sample strip $Si_3N_4$ waveguide (1000 nm × 690 nm) as shown in Figure 6a. When pumping in the anomalous GVD regime, the SCG is dominated by soliton-related propagation effects, including soliton fission, DW generation, and intrapulse Raman scattering. These phenomena play important roles when femtosecond pulses propagate through highly nonlinear media.

*Soliton Fission*: In this condition, the MI occurred when $\beta_2 < 0$, and the periodic evolution pattern would appear along propagation length, which forms the optical soliton.[42] The parameter $N$ represents the order of soliton, and the expression is given by:

$$N^2 = \frac{\gamma P_0 T_0^2}{|\beta_2|} \tag{11}$$

where $T_0$ is the width and $P_0$ is the peak power of the input pulses. The condition of $N > 1.5$ means a second- or higher-order soliton. Some higher-order effects perturb solitons for femtosecond pulses, including the parameters $\delta_3$, $s$, and $\tau_R$, represent TOD, self-steepening, and intrapulse Raman scattering, respectively. The expressions are as following:[42]

$$\delta_3 = \frac{\beta_3}{6|\beta_2| T_0} \tag{12}$$

$$s = \frac{1}{\omega_0 T_0} \tag{13}$$

$$\tau_R = \frac{T_R}{T_0} \tag{14}$$

These parameters vary inversely with pulse width and are appreciable for pulse width $T_0 < 5$ ps.[42] The perturbations could break up the high-order soliton into its constituent fundamental solitons, forming the soliton fission phenomenon.

*Dispersive Wave Generation*: When the fundamental soliton, that is, $N = 1$ is perturbed by the higher-order dispersion, a part of energy sheds to a specific frequency based on a phase-matching condition, called the DW. Such phenomenon is also known as the Cherenkov radiation or the nonsolitonic radiation (NSR), which assists in further broadening the SC spectrum. The phase-matching condition between the DW ($\omega_d$) and the soliton pulse which centered at frequency $\omega_s$ with a group velocity $v_g$ is:

$$\beta(\omega_d) = \beta(\omega_s) + \beta_1(\omega_d - \omega_s) + \frac{1}{2}\gamma P_S \equiv \eta(\omega) \tag{15}$$

where $\beta(\omega)$ is the propagation constant, $\gamma$ is the Kerr nonlinear coefficient, $P_s$ is the peak power of the soliton pulse, and $\beta_1 = 1/v_g$. DWs can be generated both in the anomalous and normal GVD regions. When pumping in the anomalous region, the normal GVD regime spectral structure or the low-amplitude temporal background can be clearly seen. This is the common feature of DW generation. DWs are usually classified into three categories: i) For $\beta_2 < 0$ and $\beta_3 > 0$, the DW is emitted at a shorter wavelength than that of the soliton. ii) For $\beta_3 < 0$, the NSR is emitted at wavelengths longer than that of the soliton. iii) For $\beta_3 = 0$, $\beta_4 > 0$, two DWs are generated simultaneously on both sides of the soliton frequency. They are denoted as SWDW and LWDW.

*Intrapulse Raman Scattering*: The noteworthy feature of intrapulse Raman scattering in the case of anomalous dispersion is the spectrum shifting toward longer wavelengths, named Raman-induced frequency shift (RIFS). In the time domain, the bent trajectory would appear. Because the energy transfer to the longer wavelength side, the group velocity is slower at longer wavelengths ($\beta_2 < 0$), and finally the propagation path is bent. The spectral shift can still occur in the normal-GVD regime where solitons are not formed. Specially, $Si_3N_4$ platform has a negligible Raman effect and lacks RIFS in the SCG.

The SC characteristics was reflected in the experiment reported by M. A. Ettabib et al[214] (**Figure 7**). In both figures, the number of DWs and soliton components could be clearly observed, through the evolution and the temporal profile along the waveguide. The order of soliton $N$ was 3, it could be seen that the high order soliton was broken off into three lower-order soliton pulses and the DWs further extended the bandwidth of the soliton-based SC to the longer wavelength region. Tuning the phase-matching wavelength of DW to be far away from the center wavelength was conducive to the broader spectra.

*Cascaded Dispersive Wave Generation*: Most of the work based on Type I dispersion focused on pumping in the anomalous-GVD regime, investigated the effect of the DW and the soliton. In the study of Y. Okawachi et al.,[270] they pumped in the normal-GVD

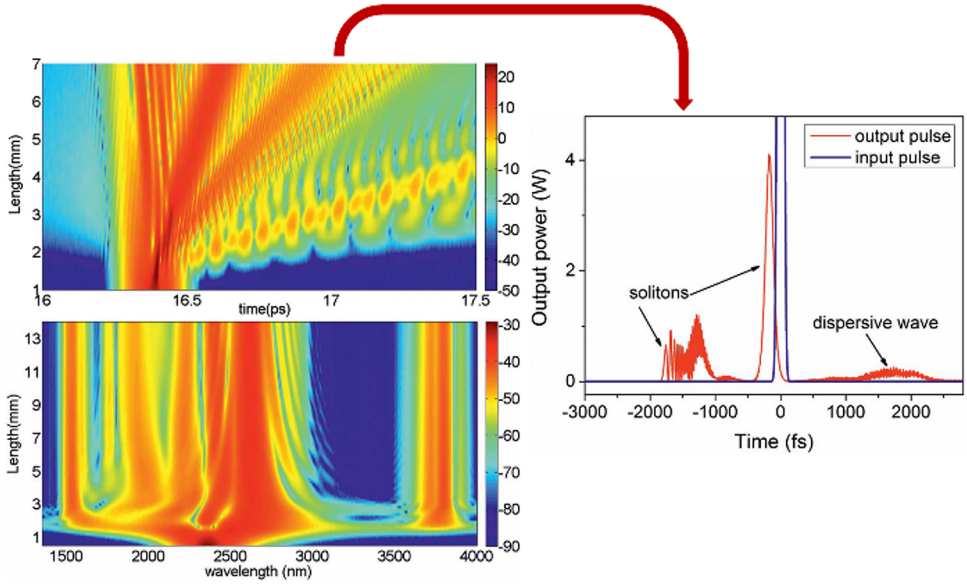


**Figure 7.** Temporal and spectral evolutions of the optical power.[214] The insert figure is the temporal profile including solitons and DWs. Adapted with permission.[214] Copyright 2015, Optica Publishing Group.

regime of Type I dispersion curve. The mechanism broadened the spectrum mainly to one side of the input pulse through the cascaded DW formation.

In this part, we compare the key SC results of various materials including experiments and simulations based on Type I. In **Figure 8**, we choose the representative experimental SC results with various materials among many works. In 2007, I.-W. Hsieh et al. observed the spectral broadening of >350 nm.[271] The experiments used single-mode Si-wire waveguides pumped at 1310 nm. L. Yin et al. showed the simulations of 500-nm bandwidth at −30 dB level, and investigated the physical process of soliton fission, SPM, and DW generation.[272] The reports from F. Leo et al.,[201] experimentally demonstrated a SC spectrum spanning from 1.17 to 1.68 μm, which first completed the characterization of SC coherence in a Si wire waveguide. The first experimental observation of DWs in a Si wire waveguide was pumped in the C-band. The DWs appeared obviously in the normal dispersion regime, and improved the bandwidth of SC spanning from 1.16 to 1.7 μm at −30 dB level.[216] In the following work, they demonstrated the bandwidth of SC spanning from 1.54 to 3.2 μm based on the similar structure, and lead to self-referenced frequency comb generation.[206] The experimental results of Si wire waveguide in 2017[222] only covered 700 nm from 1.1 to 1.8 μm at −30 dB level. The first octave-spanning SCG based on Si waveguide was demonstrated by R. K. W. Lau et al.[205] The numerical simulation of SC covered from 1.5 to 3.6 μm at −30 dB level, but the spectral flatness was not good. The cascaded waveguide proposed by C. Ciret et al. in 2016[251] and N. Singh et al. in 2019[249] provided the extra degree of freedom to optimize the properties of the SC by varying the dispersion profile. Adjusting the waveguide width along the propagation distance was a method to tailor dispersion. C. Ciret et al. designed the dispersion map using the genetic algorithm, and obtained the optimized SC covering 1.75 μm in simulation. In 2020, J. Wei et al. used more complex dispersion-managed integrated structures to generate a SC spanning from 1.9 to 2.7 μm experimentally.[252] Compared with the tapered structure and the waveguide with fixed width, the SC generated in the cascaded waveguide was slightly broader and flatter, with better coherence. N. Singh et al. discussed the properties of two cascaded waveguides, three cascaded waveguides, and the taper waveguides in experiment. To some extent, the results showed the signal enhancement and the spectra extension. However, the spectra were with significant fluctuation and the coherence decreased at both sides of the spectra. The previous experimental work of N. Singh et al. in 2018 showed the high degree of coherence over the full octave using the same Si slab waveguide, the SCG extended from 1.1 to 2.4 μm with the input pulse pumping at 1.9 μm.[226] In 2019, H. Saghaei et al. numerically investigated the SC, which spanned over 2.8 μm, using 200-fs pulses at 2.1 μm with 200-W peak power, and the spectra fluctuated significantly.[225]

To the best of our knowledge, the broadest experimental result of SOI waveguide was the study reported by R. Kou et al.[233] The proposed structure was Si rib waveguide with all-air-cladding. By tuning the waveguide dispersion parameters to obtain the flattened curve, a broad SC of 1.32 octave (2–5 μm) was observed with a 300-fs short input pulse centered at 4-μm. The length of the device was 12 mm, and the pump power was 28.8 mW. However, the spectrum of 28.8-mW pump power case was nearly identical with 12.6-mW one due to the saturation regime and the damage threshold of Si. The nonlinear absorption includes the four-photon absorption induced free-carrier absorption. Figure 8a depicts the measured spectra with two different waveguide widths ($W$) of 6 and 8 μm, including the core data generated by 8 × 2 $\mu m^2$ (slab thickness = 0.5 μm).

Different from the SOI platform, the SOS is also a viable platform for nonlinear photonics in the mid-IR. The experimental result reported by N. Singh et al.[207] in 2015 demonstrated a 1.53-octave-spanning SC in SOS nanowires, covering from 1.9 to 5.5 μm. The input pulse was centered at 3.7 μm with a 1.82-

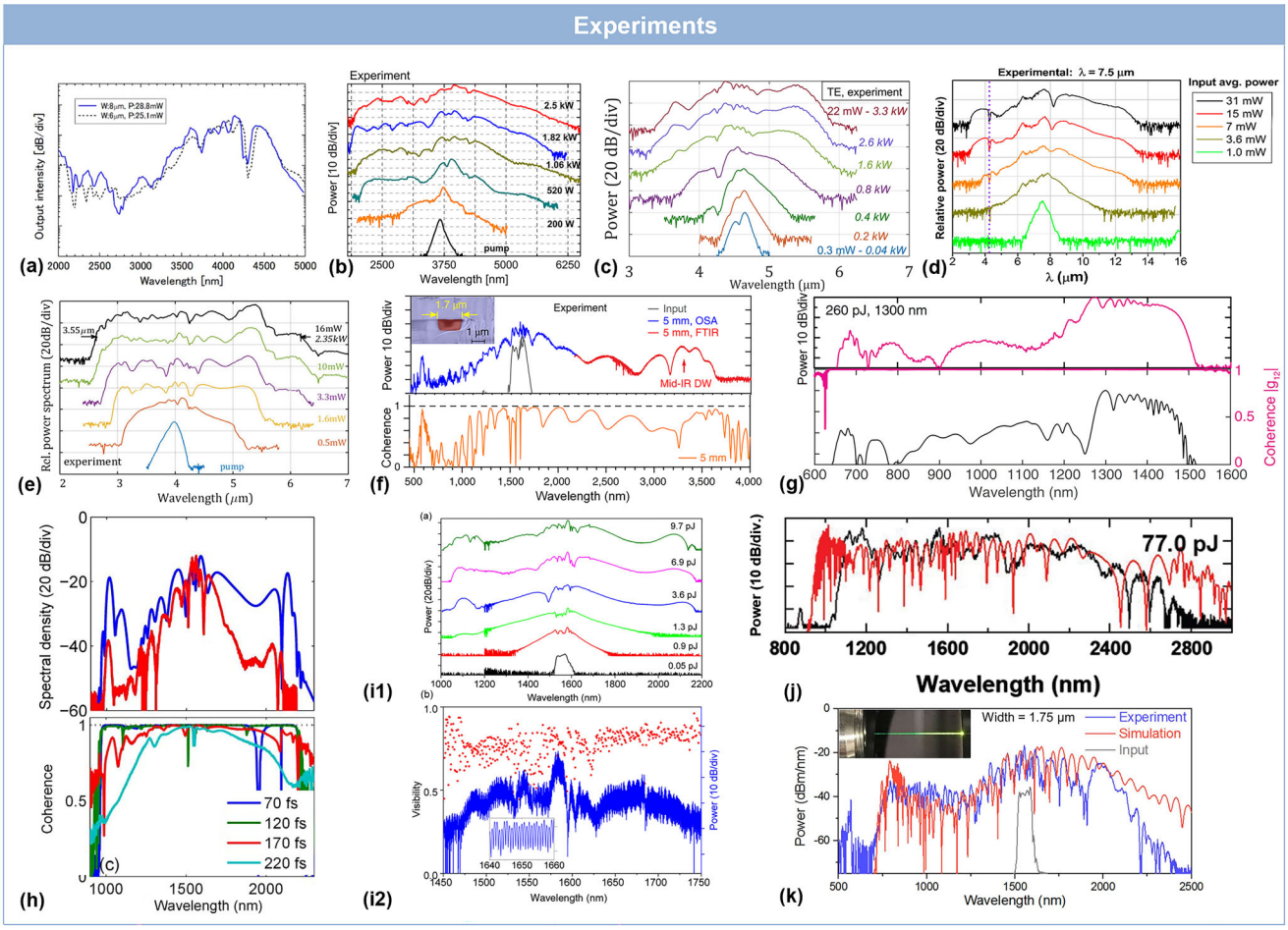


**Figure 8.** Representative experimental SCG results in the nanophotonic waveguides with different materials. a) SCG in the SOI platform with different waveguide widths and peak power.Reproduced with permission.[233] Copyright 2018, Optica Publishing Group. b) Broadest SC in SOS platform with different peak power by N. Singh et al.[207] Reproduced with permission.[207] Copyright 2015, Optica Publishing Group. c) Experimental demonstration of SCG in a Ge-on-Si waveguide by A. D. Torre et al.[265] Reproduced with permission.[265] Copyright 2021, AIP Publishing. d) SCG in $Si_{0.2}Ge_{0.8}$ waveguide with different peak powers by M. Montesinos-Ballester et al.[266] Reproduced with permission.[266] Copyright 2020, American Chemical Society. e) SCG in $Si_{0.6}Ge_{0.4}$ waveguides with different peak powers by M.Sinobad et al.[212] Reproduced with permission.[212] Copyright 2018, Optica Publishing Group. f) SCG and coherence in $Si_3N_4$ waveguides by T. J. Kippenberg et al.[39] Reproduced with permission.[39] Copyright 2018, Springer Nature. g) SC and coherence in $Si_3N_4$ waveguides pumping in normal region of Type I dispersion by Y. Okawachi et al.[270] Reproduced with permission.[270] Copyright 2017, Optica Publishing Group. h) Generated SC spectra and their corresponding coherence in InGaP waveguides with different pulse width by U. D. Dave et al.[172] Reproduced with permission.[172] Copyright 2015, Optica Publishing Group. i1) Experimental data and i2) the corresponding coherence with different energy from B. Kuyken et al. in AlGaAs waveguide.[267] Reproduced with permission.[267] Copyright 2020, Optica Publishing Group. j) SCG in $As_2S_3$ film waveguides for TM mode by J. Hwang et al.[273] Reproduced with permission.[273] Copyright 2021, Optica Publishing Group. k) Experimental and simulated spectra in the $LiNbO_3$ waveguide based on third-order nonlinearity from J. Lu et al.[145] Reproduced with permission.[145] Copyright 2019, Optica Publishing Group.

kW peak power. Furthermore, the theoretical results of generating light as far out as 8 μm demonstrated the possible SCG range in Si. This result provided the possibility to overcome the barrier of high-order multiphoton absorption in Si for the mid-IR range. N. Nader et al. in 2018[125] built the notch waveguides through the SOS platform to achieve the mid-IR frequency combs. The SC of the notch waveguide spanning from 2.5 to 6.2 μm was broader than that of the demonstrated strip waveguides without the notch.

Ge is also a Group IV photonics material, due to the wider transparent window and the larger nonlinear coefficient, which is suitable for MIR SCG. The higher-order nonlinearities including the multi-photon absorption, intrapulse Raman Scattering, FCA, and FCD effect are always considered in the simulation. Furthermore, the effects of two- and four- photon absorption are negligible compared with three-photon absorption (3PA). The 3PA was dominant to degrade the broadening of the SC. The numerical study of suspended Ge-membrane ridge waveguide to generate the MIR SC was reported by J. Yuan et al.,[232] which discussed the contribution of 3PA. The −30 dB bandwidth of the corresponding SC was about 5.04 μm covering from 1.96 to 7 μm pumped at 4.8 μm. The investigation from F. De Leonardis et al. showed the comparison for the generated SCs with or without considering the 3PA process.[218] As shown in Figure 8c, in 2020,

A. D. Torre et al. presented the first experimental demonstration of SCG in a low-loss Ge-on-Si waveguide. They injected TE and TM modes into the platform, with 3.3 and 4.5-kW peak powers, respectively. The pump wavelength resides in the normal dispersion regime for the TE mode and anomalous dispersion region for the TM mode. The generated SC of TE mode spanned from 3.53 to 5.83 μm at −30 dB level, and the one of TM mode covered from 3.33 to 5.55 μm.[265]

$Si_xGe_{1-x}$ can be used as an alternative platform to Si. The group IV alloy is also an attractive nonlinear material for mid-IR applications, which has CMOS compatibility. M. A. Ettabib et al.[214] demonstrated the broadband SCG in silicon–germanium waveguide, which adopted a graded Ge concentration profile through increasing the Ge concentration from 0% to 42%, and then reduced it back down to pure Si symmetrically. The trapezoidal structure generated the SC spanning from 1.45 to 2.79 μm (at the −30 dB level). Different from this work, M. Sinobad et al. in 2018[212] reported the SCG in an air-clad $Si_{0.6}Ge_{0.4}$ waveguide on Si, the cross-section of the waveguide was 3.75 × 2.70 $\mu m^2$, which was pumped at the anomalous dispersion regime for the TE mode. The SC spanned from 2.63 to 6.18 μm covering 3.55 μm at −30 dB level. The 200-fs input pulse was pumped at 4 μm with 2.35 kW peak power using tunable OPA. The spectra measured out of the 7 cm long waveguide is shown in Figure 8e. The spectral broadening was governed by the solitons with the order up to 20 and the DWs for the wavelength range below 3.8 μm and beyond 5.0 μm. Another waveguide design with an additional chalcogenide cladding in 2019[213] could shift the CD from anomalous to all-normal regime, which will be introduced further in the Type II dispersion section. Recently, M. Montesinos-Ballester et al. reported the experimental SCG in $Si_{0.2}Ge_{0.8}$ waveguide.[266] The waveguide is built on a $Si_{1-x}Ge_x$ buffer, with the Ge fraction x linearly increasing from 0 to 0.79. The SC was ranging from 3 to 13 μm at −30 dB level by pumping a 220-fs 9.8-kW input pulse centered at 7.5 μm, and the generated SC almost covers the full transparent window of Ge.

Specifically, $Si_3N_4$ is known for the absence of TPA in the telecom band, and its wide transparent window. Most SC generated in the $Si_3N_4$ integrated platforms can span from the visible light range. The experimental demonstration of SCG in 2012 by R. Halir et al.[274] spanned 1.6 octaves from 665 to 2025 nm in $Si_3N_4$ waveguides, which was pumped at 1.3 μm by OPO. The SC at short wavelength was broadened to the blue wavelength range (488 nm) in 2015 by H. Zhao et al.[234] The pumped wavelength emitted by the Ti:Sapphire laser was 795 nm and the −30 dB bandwidth spanned from 488 to 978 nm. The SCG extending to the infrared spectral range (2130 nm) wider than 495 THz through the $Si_3N_4$ waveguide with $SiO_2$ cladding was proposed by J. P. Epping et al.,[236] and the following report in 2017 demonstrated the measured spectra >2.5 μm spanning at least 2.2 octaves at the −30 dB level.[235] D. Martyshkin et al.[223] demonstrated the SC in longer wavelength region, that is, from 1.375 to 3.5 μm spanning more than 1.5 octaves pumped at 2.35 μm using Cr:ZnS fs oscillator. The highly coherent SC was suitable for the frequency comb offset detection using self-referencing in an f-to-2f interferometer. A. S. Mayer et al. presented the first carrier-envelope-offset frequency ($f_{CEO}$) detection of a mode-locked laser based on the $Si_3N_4$ film waveguides with $SiO_2$ cladding. The SC extended over 1.15 μm from 600 to 1750 nm,[275] and expanded to 1.3 μm in the following work.[224] In the letter of Y. Okawachi et al., they demonstrated the $f_{CEO}$ detection via the spectral overlaps between SCG and SHG. The experimental spectra showed the SCG from 657 to 1700 nm in −30 dB level.[276] A. R. Johnson et al. in 2015[200] illustrated the spectrum from 670 to 1900 nm at the −30 dB level, and measured the experimental spectral interference and visibility for coherence verification. The efficient SC spanning 700 to 2080 nm proposed by E. S. Lamb et al.[40] was broader for stabilized comb generation. D. R. Carlson et al.[217] utilized $Si_3N_4$ waveguides for telecom-wavelength frequency comb generation through 1.95-μm bandwidth SC. For multi-stage waveguide, D. D. Hickstein et al. proposed a periodic $Si_3N_4$ waveguide, which provides periodic modulations for $\gamma$ and GVD. The SC spanned from 0.5 to 2.25 μm including QPM induced DW.

Figure 8f shows the broadest experimental results for the SCG in $Si_3N_4$ waveguide, which were reported by T. J. Kippenberg et al. in 2018[39] using <90 fs pulses at 1.55 μm with 1 nJ energy. The cross-section of the $Si_3N_4$ waveguide was 0.87 × 1.7 $\mu m^2$. The corresponding spectrum covered more than two octaves, as shown in Figure 8f, spanning from 0.56 to 3.6 μm. The soliton was supported at the anomalous GVD regime, and split into three components. Two DWs were both in the normal GVD regime, residing in the visible and the mid-IR ranges, respectively. The DWs located at both edges of the spectrum. Moreover, the phase-matching wavelength of DW can be tuned by different waveguide widths. The larger cross-section was beneficial to generate the mid-IR DW at longer wavelengths. Moreover, the conversion efficiency of the mid-IR DW was degraded when it was generated at longer wavelengths. Different from the above report, the study pumping in normal dispersion were also utilized for generating the broadband SCG.[270] Y. Okawachi et al. used a 2-cm-long $Si_3N_4$ waveguide to demonstrate a SC over 657–1513 nm by generating two cascaded DWs with a 1300-nm pump. First, the spectrum was broadened due to SPM. As the input pulse propagated, the energy of pump wavelength at 1255 nm was converted to two specral components. The SWDW component is at 685 nm, and the other 1-μm component resided in the anomalous-GVD regime. This component can be regarded as the pump light of the cascade process, and subsequently generated the second DW near 740 nm. Figure 8g shows the experimentally generated SC results, where the spectral coherence is also investigated by adding the quantum shot noise. Several studies have reported some wide SCs in silicon-rich nitride platforms[277–279] by utilizing larger Kerr nonlinearity, which is two orders of magnitude larger than that in $Si_3N_4$.

Some studies used $SiO_2$ waveguide to generate the SC, due to the small Kerr coefficient of $SiO_2$, which is more than two orders of magnitude smaller than that of Si. The generated SC bandwidth in the silica waveguide is relatively narrow. In the work of D. Duchesne et al. in 2010,[181] they demonstrated a 45-cm long high-index doped silica glass spiral waveguide to improve the Kerr nonlinearity compared with the traditional silica waveguide. The spectrum was extended from 1.3 to 1.9 μm. Longer propagation length was achieved with cascaded silica interleaved waveguides in 2014, and the corresponding SCG covered 600 nm with a physical path length of 3.5 m.[95] A $SiO_2$ ridge waveguide from D. Y. Oh et al.[280] has been applied to generate the broadest SC covered 0.9 μm, and the DW was precisely tuned from UV to

visible in different channels from the waveguide array with various cross sections. The III–V materials also show the possibility to generate the SC as an on-chip III–V-based nonlinear platform, such as the InGaP and AlGaAs on-insulator waveguides reported by U. D. Dave et al. and M. Pu et al., respectively.[172,267] An InGaP waveguide on the $SiO_2$/BCB bonding layer had the high-index contrast. The Raman response was neglected in this work, and the 3PA, FCA, and FCD were considered. Figure 8h depicts the simulated (blue line) and experimental (red line) spectra. The OPO delivered pulse trains with 170-fs pulse width and 10-W peak power centered at 1.55 μm. The soliton fission and two DWs can be seen in Figure 8h. Moreover, the coherence properties in the InGaP waveguides were also studied, where the experimental method was the fringe visibility of the interference between two independent supercontinua. The coherence was better for denser interference fringes. Higher soliton number would degrade the coherence of the supercontinuum. As shown in Figure 8h, the solition number of 70-fs input pulse was 6, which was better in terms of the coherence than the 170-fs ($N \approx 15$) pulse. This investigation on the impact from the solition number could potentially guide the SCG for high coherence.

Figure 8i shows the experimental SCG result on the AlGaAsOI platform.[267] The aluminum composition of the AlGaAs layer was 21% in this work, and the nonlinear properties of AlGaAs can also be engineered by changing the Al concentration. The measured spectrum of 3-mm long AlGaAsOI waveguide with $SiO_2$ cladding is shown in Figure 8i. The SC covered 1.08 μm from 1.05 to 2.13 μm, and was generated by a 100-fs 3.6-pJ pulse. The spectra components around 1100 and 2100 nm were two DWs. When the pump pulse energy was increased, the SC spectrum started saturating due to 3PA. The experimental method for coherence measurement was also investigated. The spectral fringe after the interference showed a high contrast (10 dB), that is, a strong phase coherence. Meanwhile, the large fringe visibility of the interference pattern also indicated a good coherence of the SC.

Chalcogenide glasses are ideal candidates for planar waveguides to generate SC in the MIR, due to their large ultra-fast nonlinearity. S, Se, or Te are the common constituents of the chalcogenide glasses, which could be combined with Si, As, Ge, P, and Sb. They have the broad transparent window from near to the MIR domain. Amongst the diversified chalcogenide material systems, the commonly used chalcogenide materials include $As_2S_3$, $As_2Se_3$, $Ge_{11.5}As_{24}Se_{64.5}$ glasses. The waveguides made of these materials show some demonstrations of SCG, including $As_2S_3$ waveguides reported in 2008.[227] The 60-mm long waveguide had a 0.75-μm SC by using a 610-fs input pulse with 68-W peak power pumped TM mode at 1.55 μm. Specifically, the order of soliton was >40, and the corresponding soliton fission length was 67 mm, which was close to the device length. So the mechanism of SCG was FWM rather than soliton fission, and the idler terms could support this explanation. The measured SC spectrum was over 500 nm wide at −30 dB, which was limited by the optical spectrum analyzer in the experiment. As depicted in Figure 8j, J. Hwang et al. fabricated $As_2S_3$ film waveguides on a trapezoidal $SiO_2$ structure, which are formed automatically during the deposition process.[273] To obtain anomalous dispersion, there are certain requirements on the width and angle of the waveguide. The SC spanning from 1050 to 2710 nm at −30 dB could be obtained experimentally for the TM mode, by pumping a 502-W 135-fs input pulse centered at 1560 nm. The SC results of the TE mode were also given for comparison, and the corresponding SC covered from 1250 to 2000 nm based on the normal dispersion.

T. S. Saini et al.[230] proposed the $As_2Se_3$ chalcogenide rib waveguide with different core-shape profiles. The core was surrounded by $MgF_2$ as the lower and upper claddings due to its transparent window up to 7.7 μm. The spectrum with obviously fluctuations ranging from 1 to 12 μm was generated by a 6-mm long triangular-core waveguide in numerical modeling, when pumped with a 6.4-kW 497-fs input pulse at the pump wavelength of 2.8 μm. The As-based materials are of concern due to their toxicity and photo-darkening effect.

The specific chalcogenide glass $Ge_{11.5}As_{24}Se_{64.5}$ has the film-forming properties and high thermal and optical stability under intense illumination. From the simulations of M. R. Karim et al. in 2014,[221] they designed $Ge_{11.5}As_{24}Se_{64.5}$ nanowires with polymer cladding to reduce the index contrast between the core and cladding for suppressing the potential high-order modes. They highlighted the effects of higher-order dispersion coefficients up to $\beta_8$ terms on the SC spectrum, and higher dispersion coefficients could be included for accurate results. The generated SC had 1300-nm bandwidth. They continued to extend the SC to the MIR region in 2015,[220] by replacing the upper claddings with air and choosing $Ge_{11.5}As_{24}S_{64.5}$ glass as the lower cladding material. The simulated SC expanded to 4-μm spectral range from 2 to 6 μm for a 3.1-μm input pulse. When $MgF_2$ glass acted as lower cladding, the SC was extended from 1.8 to 10.1 μm, and the −30 dB bandwidth was 8.3 μm. Y. Yu et al.[173] reported a $Ge_{11.5}As_{24}Se_{64.5}$ rib glass on a $Ge_{11.5}As_{24}S_{64.5}$ bottom cladding with an air upper cladding, which could extend the SC spectrum from 1.8 to 8 μm at -30 dB level using the OPA of 4-μm 320-fs duration pump pulses. Specifically, the bottom cladding was with a fluoropolymer protective coating to prevent the surface contamination. The following reports[229] overcame the long wavelength limit of the spectrum due to the asymmetry between the upper air cladding and the bottom fluoropolymer cladding. The upper air cladding was replaced by $Ge_{11.5}As_{24}S_{64.5}$ and the experimental SC spectrum covered from 2.2 to 10.2 μm at −30 dB for the TM mode. The DWs were at around 3 and 8 μm, respectively. A 330-fs 4500-W pump pulse was chosen at 4.184 μm from an OPA system. This is the best experimental report so far for SCG using chalcogenide glass waveguides. The $Ge_{23}Sb_7S_{70}$ waveguide cannot be oxidized in air and do not have any photo-darkening effect either. J.-É. Tremblay et al.[162] demonstrated a $Ge_{23}Sb_7S_{70}$ waveguide pumped at 1.55 μm, and the SCG extended from 1.03 to 2.08 μm with a 26-pJ pulse energy. In 2021, H. Shang et al.[281] generated SC spectrum covering from 850 to 2150 nm in a $Ge_{23}Sb_7S_{70}$ strip waveguide, by pumping a 290-fs 7.46-kW input pulse. The center wavelength of the pump was 1550 nm.

Although some alternative platforms exhibit large nonlinear refractive index, there are still not being widely used for SCG until now. For example, the nonlinear refractive indices of $TaFD_5$, $Ta_2O_5$, $TiO_2$, graphene, and a:Si-H are much larger than silica. I. Babushkin et al.[231] predicted and numerically studied the SCG of the $TaFD_5$ glass rib waveguide on the $SiO_2$. A fluctuant SC was obtained extending from 750 to 2400 nm, and the temporal field distribution exhibited many spikes corresponding to the fundamental solitons with different frequencies. The DW

generation based on the phase-matching condition also can be observed. In 2017, they obtained the SCG generated in an $TaFD_5$ glass array.[113] The spectrum extending from 500 to 3000 nm showed severe fluctuation. R. Fan et al. used $Ta_2O_5$ waveguide to realize SCG ranging from 565 to 1464 nm at −30 dB pumped by a mode-locked laser at 1056 nm.[112] The material is suitable to be fabricated as the optical waveguide cores due to the small extinction coefficient and thermal-optical coefficient. J. R. C. Woods et al. presented the SCG in a $Ta_2O_5$ waveguide with or without $SiO_2$ cladding. They demonstrated the broadest SC expanding from 750 to 1300 nm at −30 dB in a $SiO_2$-cladded waveguide for the TM mode. They also showed the experimental SC results for higher order modes in both the TE and TM polarizations.[282] K. F. Lamee et al. experimentally demonstrated the SCG in $Ta_2O_5$ waveguides with air or $SiO_2$ cladding.[269] The SC covered from 620 to 2350 nm including SWDW generation at 640 nm in the air-cladding $Ta_2O_5$ waveguide, and the SC generated in the $SiO_2$ cladding waveguide spanned from 680 to 2420 nm containing SWDW at 700 nm, by pumping an 80-fs pulses with a center wavelength of 1560 nm. Except for the high nonlinear refractive indices, a wider band gap and better thermo-optical stability are also the advantages of $TiO_2$. H. Ryu et al. in 2012 examined the waveguide dispersion of slot waveguides by analyzing the index contrast. In the following study, SC was achieved using the $TiO_2$ core with $Ta_2O_5$ slot and $SiO_2$ cladding. Based on the anomalous dispersion, the spectrum broadened from 600 nm to 1.4 μm was observed and the coherence was quite low and fluctuant.[241] In 2018, the SC achieved by K. Hammani et al. expanded from the visible wavelength to the MIR region covering 1.25 μm at −30 dB with anomalous dispersion.[111] S. S. Bobba et al.[283] proposed the ridge waveguides consisting of a single, bi-or tri-layer of Graphene on the $SiO_2$ substrate with the $Si_3N_4$ hexagonal crystalline outer core to obtain the SC. The designed waveguide produced the broadest SC to the best of our knowledge ranging from 1.5 to 25 μm with a low input peak power of 1 W. Thanks to the favorable properties of a-Si:H waveguides, there are some reports generating the broad SC by pumping picosecond pulses. F. Leo et al. studied the SCG seeded by 180-fs, 13-W peak power input pulse centered at 1575 nm.[268] The SC spectrum spanned from 1410 to 1940 nm at −30 dB. The advantage of a-Si:H waveguide for SCG was proven compared with the c-Si waveguide.

Previous demonstrations in $LiNbO_3$ have shown the applications based on the stronger $\chi^{(2)}$ nonlinearity, such as the SH and the SC generated in high $\chi^{(2)}$ waveguides. The spectrum was broadened from 0.7 to 2.2 μm at −30 dB by J. Lu et al.[145] As shown in Figure 8k, the green light occurred due to THG, and then soliton fission emerged, which was illustrated by the green to yellow color changing along the propagation. M. Yu et al. demonstrated the SCG in a $LiNbO_3$ waveguide including a DW near 800 nm and the spectrum was broadened around the pump wavelength due to SPM.[237] The experimental results showed a 1.5-μm SC bandwidth from 0.75 to 2.25 μm at −30 dB, and the coherence was near 1 over most of the generated SC range based on 128 individual simulations. Specially, the SHG components also broadened the spectrum, and SFG between the SCG and SHG components was obtained. In addition to the single $LiNbO_3$ waveguide, PPLN is also a candidate to generate SC through the $\chi^{(2)}$ nonlinearities. C. R. Phillips et al.[252] generated a 2.2-μm SC by using PPLN.

Aluminum nitride (AlN) is also an integrated material exhibiting both strong $\chi^{(2)}$ and $\chi^{(3)}$ with a broad transparent window. H. Chen et al. explored the SCG covering from near-UV to near-IR using AlN waveguides on sapphire substrates.[238] In this case, a high order waveguide mode ($TE_{10}$) was used for anomalous dispersion. The main spectrum of the generated SC was generated by soliton fission and DW, which covered from 650 to 950 nm. The secondary spectrum was broadened by SHG spanning from 405 to 425 nm. There were obvious fluctuations in the SC coherence. D. D. Hickstein et al. achieved the SC from 700 to 4000 nm pumped in $TE_{00}$ mode using AlN waveguides.[239] The blue side and the red side of the spectrum had the SWDW and LWDW, respectively. While the AlN films used in this study had a strong $\chi^{(2)}$ component in the vertical (TM) direction. They also observed the SHG, difference frequency generation (DFG) and THG due to the strong $\chi^{(2)}$ effects in the $TM_{00}$ mode. J. Lu et al. reported the SCG spanning from 700 to 3600 nm at −30 dB in AlN waveguides.[284] The recorded DWs were located at 750 and 3700 nm, respectively. At the same time, the narrow-band blue light induced by THG at 500 nm was recorded under TE polarization. Under a TM pump, cascaded SHG was observed from near-visible to even UV regime.

**Table 2** shows the summary of the broadest experimental SCG results in the nanophotonic uniform waveguides with different materials, including the key factors that impact the spectral broadening, such as the CD value and nonlinear coefficient. The propagation length $L$ of the waveguides provides length scales for dispersive and nonlinear effects relative magnitudes. The basic information of the input pulse was also studied, such as the FWHM, the peak power and the pump wavelength of the input pulse. Furthermore, superscript "a" represents the parameters that are not directly mentioned in the paper. We extracted the relevant information and diagrams, and then calculated the parameters with the superscript "a." The −30 dB level bandwidth represents the spectral range from the maximum intensity point to −30 dB point. The star sign in the "Bandwidth −30 dB level" column indicates the spectra with obviously intensity fluctuations, and there are the frequency components below the −30 dB level from the base line.

#### 5.2.2. All-Normal Dispersion (Type II)

We further investigate the waveguides with all-normal dispersion as shown in Figure 6. The nonlinear effects mentioned above, such as soliton fission and DWs generation that require anomalous dispersion, are not taken into consideration. SPM, self-steepening, and OWB are the main possible mechanisms for SCG with all-normal dispersion.

*Self-Phase Modulation*: SPM generates the new frequency components continuously when the input pulse propagates along the waveguide. In the case of unchirped pulses, the SPM-generated frequency components could broaden the spectrum. The most obvious feature of SPM is the oscillatory structure with multiple peaks. The new frequency components are red-shifted near the leading edge and blue-shifted near the trailing edge of the pulse. Due to the normal-dispersion, the red-shifted components travel faster than the blue ones. Compared with the case considering the GVD alone, the pulse walks off faster in the time

**Table 2.** Significant parameters in SCG process of waveguides with various materials based on convex anomalous dispersion (Type I).

| Material and reference | Length [mm] | Dispersion at pump wavelength [ps nm$^{-1}$ km$^{-1}$] | $\gamma$ at pump wavelength [m W$^{-1}$] | Center wavelength [μm] | Pulse width [fs] | Peak power [kW] | Bandwidth @ −30 dB level [μm] |
|---|---|---|---|---|---|---|---|
| $Si_3N_4$[39] | 5 | 126.63[a)] | 0.82[a)] | 1.55 | <90 | >11 | 3.04* |
| Si on sapphire[207] | 16[a)] | 10 | 8.86[a)] | 3.7 | 320 | 1.82 | 3.6 |
| Si[233] | 12 | 100 | 0.41[a)] | 4 | 300 | 96 | 3 |
| $SiO_2$[280] | 15 | \ | 0.038[a)] | 1.064 | 90 | 25.56 | 0.9* |
| $Si_{0.6}Ge_{0.4}$[212] | 70 | 6 | 0.63 | 4 | 200 | 2.35 | 3.55 |
| $Si_{0.2}Ge_{0.8}$[266] | 5.5 | 20 | 0.5 | 7.5 | 220 | 9.8 | 10 |
| Ge on Si[265] | 22 | 10 | 1.65 | 4.6 | 200 | 4.5 | 2.22 |
| InGaP[172] | 2 | 470.74 | 450 | 1.55 | 170 | 0.01 | 1.1* |
| AlGaAs[267] | 3 | 700 | 630 | 1.55 | 100 | 0.036 | 1.08* |
| $As_2S_3$[273] | 10 | 100 | 11.1 | 1.56 | 135 | 0.502 | 1.66 |
| GeAsSe[229] | 18 | 5[a)] | 0.2 | 4.184 | 330 | 4.5 | 8 |
| GeSbS[162] | 20 | 90 | 7 | 1.55 | 240 | 0.77 | 1.05 |
| $Ge_{25}Sb_{10}S_{65}$[281] | 9 | 250 | \ | 1.55 | 290 | 7.46 | 1.3 |
| $Ta_2O_5$[269] | 13.4 | 100 | \ | 1.56 | 80 | 10[a)] | 1.74 |
| $TaFD_5$[113] | 50 | 36.8 | 0.039[a)] | 1.6 | 200 | 40[a)] | 2.5* |
| $TiO_2$[111] | 22 | 20 | 1.2 | 1.64 | 90 | 1.78 | 1.25* |
| Graphene[283] | 1 | 837.9 | 530 000 | 1.55 | 1 | 0.001 | 23.5 |
| a:Si-H[268] | 10 | 2589 | 740 | 1.575 | 180 | 0.013 | 0.53* |
| $LiNbO_3$[145] | 10 | 160[a)] | 0.4 | 1.56 | 200 | 4 | 1.5* |
| AlN[239] | 10 | \ | 0.36[a)] | 1.56 | 80 | 10 | 3.3* |

[a)] Represents the parameters we simulated indirectly; Table only shows the broadest results with anomalous dispersion; *Represents the spectral bandwidth with obviously fluctuations.

domain. Thus, it is more difficult to generate a broadband SC in an all-normal GVD ($\beta_2 > 0$) waveguide, especially compared with the bandwidth of the SC based on the anomalous dispersion.

*Optical Wave-Breaking*: Compared with the carrier frequencies, that is, the center wavelength of the input pulse, the SPM-generated red-shifted frequencies at the leading edge ($T < 0$) move faster, and blue-shifted frequencies at the trailing edge move slower due to the effect of all-normal-dispersion. The faster red-shifted light near the leading edge overtakes the original carrier wave, that is, the faster red-shifted section takes over the slower leading edge tail. In the temporal domain, two different frequencies overlap in the pulse tails and then generate new frequencies through interference. The phenomena origin from the oscillations at the pulse edge, and the progress is defined as OWB.[285] **Figure 9**a,b shows the spectral and temporal evolutions including OWB.[140]

The FROG traces simulation from C. Finot et al. demonstrated the OWB process,[286] and we further mark the details in Figure 9c–f to make it easier to understand. Figure 9c–f could be obtained from a cross-correlation frequency resolved optical gating device, which shows the temporal and frequency evolutions at the same time. The white dotted line represents the carrier wave, and the key changes are indicated by arrows.

The group velocity of the pulse is inversely proportional with the intensity, and the peak of pulse moves slower than the tails. The pulse becomes asymmetric due to the peak shifting toward the trailing edge, and results in a steep trailing edge in the time domain. The process is called self-steepening effect, and another feature is the asymmetry in frequency domain, the spectral broadening is larger at short wavelengths than the long wavelength side due to the steeper trailing edge.

We summarize the reports of various materials based on all-normal dispersion. Compared with the SCG results with anomalous dispersion, the demonstrations of Type II dispersion are much less, especially for the experimental reports. The bandwidth of SC with all-normal dispersion is usually not satisfactory, because the SPM-induced broadening is narrower, and the soliton fission and DW do not occur. Nevertheless, the high coherence is the distinct advantage of SC generated in the normal-GVD regime. We summarize the previous reports including experiments and simulations in **Figure 10**.

C. Bao et al. proposed the horizontal double-slot Si waveguide,[242] which generated the SC with flat-top profile and the -30 dB bandwidth spanning from 1450 to 2000 nm in simulation. The SC was smooth and narrow, as it was mainly formed by SPM broadening. The peak power of the input pulse was 15 W and the center wavelength was 1.7 μm. The energy was relative low, thus there is potential to further improve this result and obtain a broader SC spectrum using an input pulse with higher peak power. The numerical simulation from H. Saghaei et al. also proposed the side-slotted waveguide to obtain the SC from 1.15 to 3 μm.[225] By pumping a 200-fs 200-W peak power input pulse at 2.1 μm wavelength. Compared with pumping a standard SOI strip waveguide in the anomalous dispersion regime with the same input pulse, the SC spectrum was a relatively smooth but narrower.

E. Tagkoudid et al. demonstrated the extreme polarization-sensitive dynamics of SCG experimentally, and the correspond-

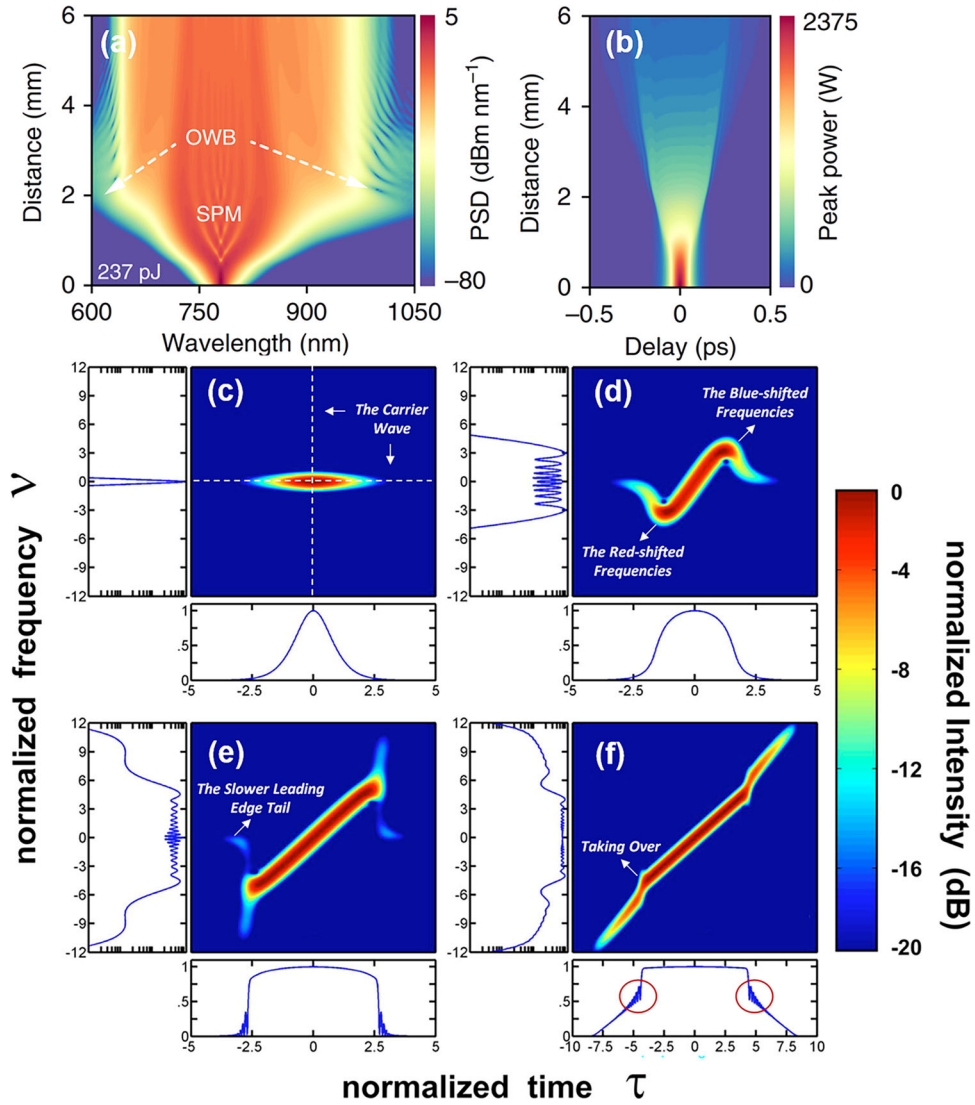


**Figure 9.** a,b) Spectral and temporal evolutions of the AlN waveguide from X. Liu et al. as the schematic of OWB.[140] Adapted with permission.[140] Copyright 2019, Springer Nature. c–f) Using the FROG traces simulation from C. Finot et al. to explain the OWB process.[286] Adapted with permission.[286] Copyright 2008, Optica Publishing Group.

ing bandwidth of SC with all-normal dispersion is 700 nm.[288] L. Zhang et al. showed the simulated SCG based on $Si_3N_4$ slot waveguide.[240] The obtained dispersion was normal at all wavelengths, and the SC was from 630 to 2650 nm at −30 dB, covering a two-octave bandwidth. The broadening mechanism was SPM together with the self-steepening effect. Moreover, they observed the steep trailing edge of the pulse that was as short as 3 fs due to the self-steepening. The output pulse showed the fluctuation at the tail in the time domain, which seems to be original from the OWB.

M. Sinobad et al. compared different dispersion properties in various $Si_{0.6}Ge_{0.4}$ waveguide structures.[212] In the demonstration of 2018, the waveguide with 3.75 μm × 2.70 μm was pumped at anomalous dispersion regime, and the generated SC spanned over 3.55 μm. In 2019, they further investigated the $Si_{0.6}Ge_{0.4}$ with chalcogenide $Ge_{11.5}As_{24}Se_{64.5}$ cladding deposited by thermal evaporation.[213] Adding the chalcogenide cladding made all-normal dispersion, the SC spanned from 3.1 to 5.5 μm at −30 dB level. One can see that it is possible to tailor the dispersion profile by adding a chalcogenide cladding layer on the original waveguide design, and the SC dynamics was also changed accordingly. Recently, they obtained an all-normal dispersion based on the wider $Si_{0.6}Ge_{0.4}$ waveguide with air cladding.[287] They experimentally demonstrated a MIR SC extending from 2.8 to 5.7 μm by pumping a 205-fs pulse residing around 4 μm at −30 dB level, and showed the calculated high-level coherence of the SC.

The report from M. R. E. Lamont et al. also demonstrated the $As_2S_3$ waveguide with all-normal dispersion based on the orthogonally-polarized mode, that is, TE mode.[227] The dispersion was negative over the whole wavelength range and $D$ equals to −210 ps nm$^{-1}$ km$^{-1}$ at $\lambda = 1550$ nm. From Figure 10d, a narrow spectrum generated by normal dispersion was compared with the soliton-induced SC spectra in $As_2S_3$ film waveguides, and the

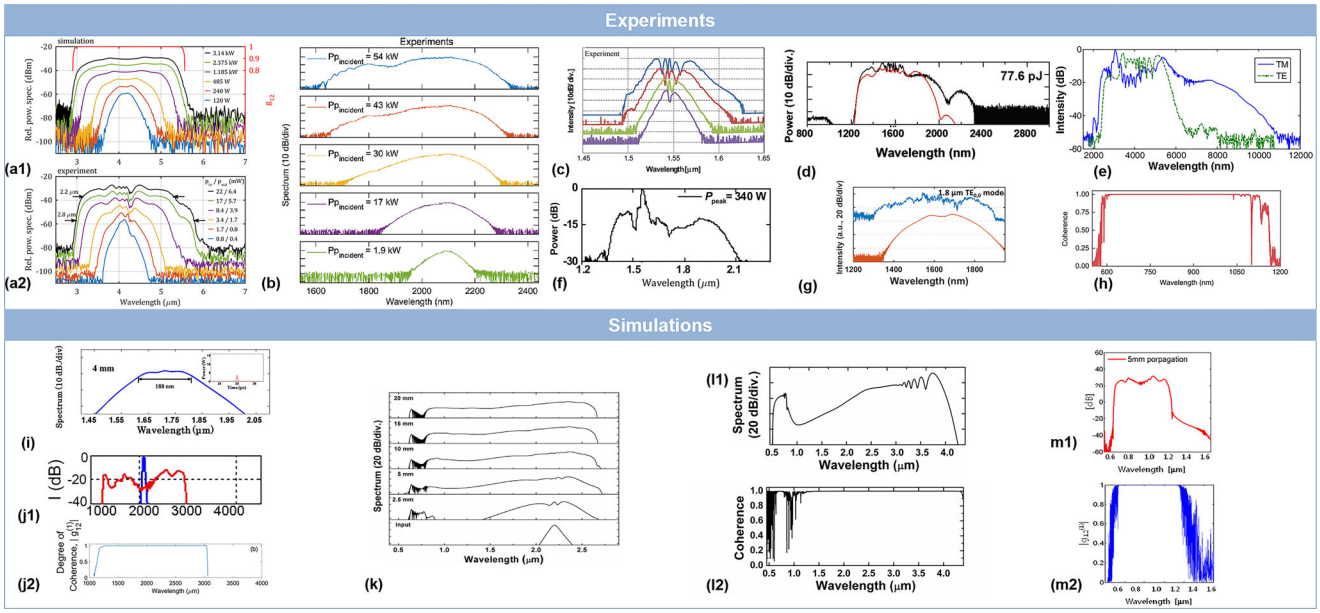


**Figure 10.** Experiment and simulation results with Type II dispersion. a1) Measured, a2) simulated SC and the coherence for the TM mode in $Si_{0.6}Ge_{0.4}$ waveguide with air cladding from M. Sinobad et al.[287] Reproduced with permission.[287] Copyright 2020, Optica Publishing Group. b) Experimental SCG in $Si_3N_4$ waveguide for TM mode as increasing incident peak power from E. Tagkoudi et al.[288] Reproduced with permission.[288] Copyright 2021, Optica Publishing Group. c) Experimental SC spectra of different peak powers for the TE mode in the $As_2S_3$ rib waveguide from M. R. E. Lamont et al.[227] Reproduced with permission.[227] Copyright 2008, Optica Publishing Group. d) SC spectra in the $As_2S_3$ film waveguides from J. Hwang et al.[273] Reproduced with permission.[273] Copyright 2021, Optica Publishing Group. e) Spectrum of TE mode through $Ge_{11.5}As_{24}Se_{64.5}$ glass by Y. Yu et al.[229] Reproduced with permission.[229] Copyright 2016, Optica Publishing Group. f) SC from J. W. Choi et al. using $Ge_{23}Sb_7S_{70}$ ridge waveguide.[101] Reproduced with permission.[101] Copyright 2016, Springer Nature. g) $TiO_2$ waveguide with 1.8 μm width featuring the all-normal dispersion from K. Hammani et al.[111] Reproduced with permission.[111] Copyright 2018, Multidisciplinary Digital Publishing Institute. h) Coherence of spectrum components relied on the $\chi^{(3)}$ nonlinear process by using AlN waveguide from X. Liu et al.[140] Reproduced with permission.[140] 2019, Springer Nature. i) Flat-top SC generated in double-slot Si waveguide from C. Bao et al.[242] Reproduced with permission.[242] Copyright 2015, Optica Publishing Group. j1) SC and j2) coherence of Si side-slotted waveguide from H. Saghaei et al.[225] Reproduced with permission.[225] Copyright 2019, Optica Publishing Group. k) Simulated SCG based on $Si_3N_4$ slot waveguide along the propagation from L. Zhang et al.[240] Reproduced with permission.[240] Copyright 2011, Optica Publishing Group. l1) Generated SC and l2) coherence of $Si_3N_4$ horizontal slot waveguide from our work. m1) Spectrum and m2) coherence using $TiO_2$ core waveguide with $Ta_2O_5$ slot from H. Ryu et al.[241] Reproduced with permission.[241] Copyright 2012, Optica Publishing Group.

SC induced by SPM and Raman effects extended from 1250 to 2000 nm.[273]

Y. Yu et al. verified the SCG through $Ge_{11.5}As_{24}Se_{64.5}$ glass in the condition of all-normal dispersion. They measured the spectrum of the TE mode with the same input pulse.[229] Compared with the SC caused by anomalous dispersion, the spectrum was from 2.2 to 6 μm. The Ge—Sb—S system (GeSbS) has been widely investigated for nonlinearity optical applications. $Ge_{23}Sb_7S_{70}$ is one of the promising waveguide materials due to its low toxicity, compared with the As-based chalcogenide glasses. J. W. Choi et al. studied the $Ge_{23}Sb_7S_{70}$ ridge waveguide on the $SiO_2$ substrate.[101] The input laser was centered at 1550 nm, and the SPM-induced spectral broadening was from 1280 to 2120 nm at −30 dB level experimentally. The report of H. Ryu et al. in 2012[241] also examined the SCG in all-normal dispersion regime using $TiO_2$ core waveguide. By tailoring the slot thickness to get all-normal dispersion, the coherence was much improved, but the SC range was only from 0.523 to 1.226 μm. In 2018, K. Hammani et al. also discussed the waveguide with 1.8 μm width featuring the all-normal dispersion, the spectrum was obviously narrower and flattened.[111]

X. Liu et al. exploited the AlN chirp-modulated taper waveguide, which included multiple length-distinct linear-taper segments.[140] The spectrum components at near-visible regime from 678 to 882 nm were generated by SPM and OWB. The spectral components at UV wavelength relied on the $\chi^{(2)}$ nonlinear process, that is, SHG and SFG by engineering the QPM condition.

In the following part, we introduce our work based on the $Si_3N_4$ horizontal slot waveguide with $SiO_2$ cladding to generate SC in Figure 10l.[246] The proposed waveguide produces an average CD of −15.56 ps (nm km)$^{-1}$ over a 3270-nm wavelength range from 1170 to 4440 nm, which covers a 1.9 octave-spanning wavelength range. To our knowledge, it is the broadest flattened dispersion curve ever reported. For a 100-fs 90-kW pulse with a center wavelength of 3200 nm, the SC spectrum expands from 504 to 4229 nm at −40 dB, covering a record-high three-octave bandwidth. The coherence is >0.99 from 1250 to 4300 nm, as the spectrum in this region is mainly expanded by the SPM, OWB and self-steepening effects.

**Table 3** shows the summary of the experiment and simulation results based on all-normal dispersion by using nanophotonic waveguides with different materials. There are fewer reports and the broadest SC is formed by GeAsSe waveguide, and the bandwidth of SC is 3.8 μm at −30 dB level, which is narrower than the SCG with anomalous dispersion shown in Table 2. There is no

**Table 3.** Key parameters in the SCG process of waveguides with various materials based on all-normal dispersion (Type II); Table shows all the results with all-normal dispersion.

| Material and reference | Length [mm] | Dispersion at pump wavelength [ps $nm^{-1}$ $km^{-1}$] | $\gamma$ at pump wavelength [$m\ W^{-1}$] | Center wavelength [μm] | Pulse width [fs] | Peak power [kW] | Bandwidth @ −30 dB level [μm] | Octave @ -30 dB level |
|---|---|---|---|---|---|---|---|---|
| $Si_3N_4$[240] | 15 | −50[a)] | 0.49 | 2.2 | 120 | 6 | 2.02 | 2.07 |
| $Si_3N_4$[246] | 5 | −19.80 | 0.12 | 3.2 | 100 | 90 | 2.825 | 1.65 |
| Si[242] | 4 | −18[a)] | 102 | 1.7 | 50 | 0.015 | 0.55 | 0.46 |
| Si[225] | 10 | −0.07 | 85 | 2.1 | 200 | 0.2 | 1.85 | 1.38 |
| $Si_{0.6}Ge_{0.4}$[213] | 70 | −12 | 0.3 | 4.15 | 200 | 3.54 | 2.4 | 0.83 |
| $S_{i0.6}Ge_{0.4}$[287] | 70 | −12 | 0.8 | 4.15 | 205 | 3.14 | 2.8 | 0.95 |
| $As_2S_3$[227] | 60 | −210 | 10 | 1.55 | 610 | 0.055 | 0.1 | 0.09 |
| $As_2S_3$[273] | 10 | −120 | 11.1 | 1.56 | 135 | 0.506[a)] | 0.75 | 0.68 |
| GeAsSe[229] | 18 | −10[a)] | 0.2 | 4.184 | 330 | 4.5 | 3.8 | 1.45 |
| GeSbS[101] | 15 | −60 | 7 | 1.55 | 500 | 0.34 | 0.84 | 0.73 |
| $TiO_2$[111] | 22 | −95 | 1.2 | 1.64 | 90 | 1.3 | 0.55 | 0.51 |
| $TiO_2$[241] | 5 | −0.05 | 12.76 | 0.8 | 100 | 1 | 0.703 | 1 |
| AlN[140] | 6 | −0.67 | 9.5 | 0.78 | 100 | 2.37 | 0.204 | 0.38 |

[a)] Represents the parameters we calculated indirectly.

star sign in the "Bandwidth @ −30 dB level" column, which indicates the spectra without obviously intensity fluctuations, and confirm to the characteristic of SCG with all-normal dispersion. Additionally, almost all the results are less than two octave spanning due to the limitation of spectral broadening mechanism. This is another potential research area for SCG in the future.

#### *5.2.3. Dispersion with Multiple Zero-Dispersion Wavelengths (Type III)*

The strong CD makes the new frequencies generated by nonlinear processes walk off quickly and suppresses the SC broadening. Some reports achieve the flattened and near-zero dispersion through tailoring the CD with multiple ZDWs, and they are even more suitable for SCG. Figure 6c is the diagram of the multiple ZDWs dispersion, that is, Type III. The existed demonstrations of SCG based on Type III are all numerical results, and the investigations of SCG in the following part are all based on the dispersion with 4 ZDWs. Recently, the flattening dispersion profiles with 5 or 6 ZDWs[244] were also obtained. They introduced the double slot layers on a slab structure with cladding, but they have not yet further investigated the nonlinearity applications. Consequently, there is also an opportunity to explore the phenomena and mechanisms of SCG behind.

L. Zhang et al. proposed the Si waveguide with four ZDWs for the first time in 2012.[128] The dispersion fluctuated between −22 and +20 ps $(nm{\cdot}km)^{-1}$ over a 667-nm bandwidth. The pump wavelength was 1810 nm within the anomalous dispersion region. The simulated SC bandwidth was 1250 nm, ranging from 1200 to 2450 nm. The output pulse was compressed to 10.1 fs due to the broadening of spectrum. **Figure 11**a shows the simulation results of another report based on the same structure.[129] The SC was up to 2464 nm, and the pulse was compressed down to 12 fs. The beating patterns at the rising and falling edges of the pulse were from the LWDW and SWDW, respectively. The vertical double slots Si waveguide also exhibited the flat and low dispersion with four ZDWs proposed by M. Zhu et al.[127] The material of vertical slot was silicon nanocrystals (Si-nc). The flattened dispersion was between −24 and +22 ps/(nm·km) from 1527 to 2625 nm over a 1098-nm bandwidth. The corresponding SC was 1630 nm. N. Singh et al. designed the waveguide with special upright-T and inverted-L structures on the sapphire substrate,[126] which could suppress the losses induced by the substrate. The dispersion varied from −25 to 25 ps $(nm{\cdot}km)^{-1}$ over 2.8 μm for upright-T waveguide, and the dispersion fluctuated from −29 to +29 ps $(nm{\cdot}km)^{-1}$ covering 4.1 μm for inverted-L waveguide. The dispersion curves all had four ZDWs. The extended SC spectrum of the inverted-L waveguide was from 2.7 to 7.5 μm at −30 dB level, and the bandwidth of the SC spectrum from the upright-T waveguide was broader but with more fluctuations.

M. Yang and L. Zhang et al. further demonstrated the dispersion engineering with four ZDWs using the suspended Ge-on-Si waveguide.[289] The Ge strip waveguide was on the suspended Si membrane, and the suspended structure without $SiO_2$ substrate could reduce the leakage loss. The dispersion varied from +9.45 to +51 ps $(nm{\cdot}km)^{-1}$ covering 7.06 μm. The broadened spectrum was from 3.7 to 9.24 μm at −30 dB level with perfect coherence after the 6.57-μm centered input pulse propagating 5.35 mm.

## 6. Supercontinuum Generation Based on Second-Order Nonlinearity

The SCG processes can also be achieved in waveguides with large second-order nonlinearities. The high nonlinear interactions only need few-nanojoule pump sources. The soliton-induced SCG depends on the reaction between the anomalous dispersion and the third-order Kerr self-focusing nonlinearity. Different from that, the quadratic nonlinear waveguides such as the standard $LiNbO_3$ or AlN waveguide generate the SC mainly based on

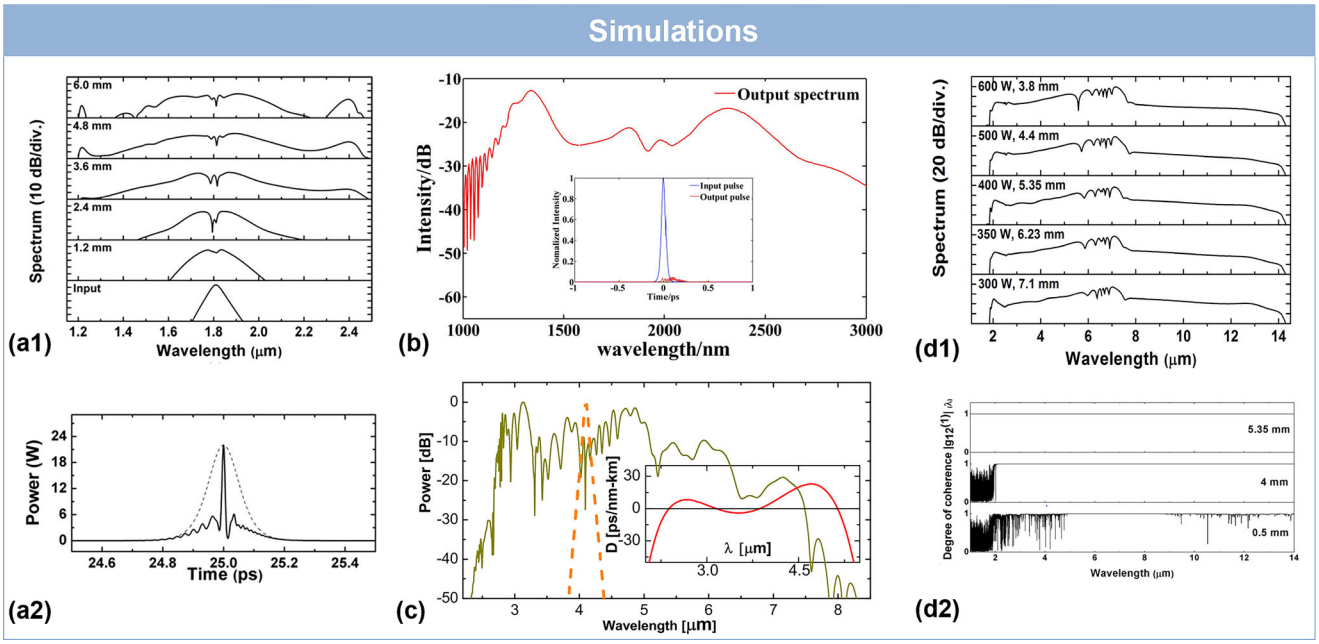


**Figure 11.** Demonstrations of SCG based on Type III dispersion. a1) Pulse spectra and a2) waveforms of Si waveguide with four ZDWs from L. Zhang et al.[129] Reproduced with permission.[129] Copyright 2012, IEEE. b) Spectral profile and temporal shape of vertical double slots Si waveguide proposed by M. Zhu et al.[127] Reproduced with permission.[127] Copyright 2012, Optica Publishing Group. c) Spectrum and corresponding dispersion curve of Si waveguide with special inverted-L structures on the sapphire substrate designed by N. Singh et al.[126] Reproduced with permission.[126] Copyright 2015, Optica Publishing Group. d1) SC and d2) coherence of suspended Ge-on-Si waveguide demonstrated by M. Yang and L. Zhang et al.[289] Reproduced with permission.[289] Copyright 2017, Optica Publishing Group.

the cascaded nonlinearities. The cascaded nonlinearities act like a cubic Kerr nonlinearity and the process can be expressed by:[290]

$$n_2^{\text{cascade}} \propto -\frac{d_{\text{neff}}^2}{\Delta k} \tag{16}$$

where $\Delta k$ is the phase-mismatch, $d_{\text{eff}}$ represents the effective quadratic nonlinearity. In previous reports, the QPM condition is used to reduce $\Delta k$ and enhance cascading progress.[256,291,292] Meanwhile, $d_{\text{eff}}$ decreases faster.[293] In the following demonstrations, the more efficient method for cascaded nonlinearity is phase-mismatched,[294,295] which generated the cascaded phase shift and resulted in the spectral broadening in the QPM waveguides. Under the strong phase-mismatched conditions, the self-defocusing soliton compression would occur and lead to the spectrum broadening effectively. The formation of self-defocusing soliton could generate the SC in normal dispersion regime. The mechanism is the interaction of cascaded $\chi^{(2)}$ process and normal dispersion.

C. Langrock et al. observed SHG and THG in the visible and near-infrared using PPLN.[292] The DFG was also obtained at the wavelength near to the zero SHG group velocity mismatch. They demonstrated the chirped PPLN devices having the advantages of spectral broadening. The broadening mechanism was explored in 2011,[295] with the consideration of $\chi^{(2)}$ nonlinearities, $\chi^{(3)}$ nonlinearities, and SRS for SCG. The modelling agreed well with the experimental results. They discussed the relationship and the contribution of cascaded $\chi^{(2)}$ and $\chi^{(3)}$ within the experimental results in details. H. Guo et al. obtained the SC through the $LiNbO_3$ waveguide which supported the self-defocusing soliton compression.[294] In the following reports,[296] the spectrum was broadened in the blue edge induced by the self-defocusing nonlinearities, and the red-edge frequency components were generated by the DW generation. Overall, the SCG in the $LiNbO_3$ ridge waveguide utilizes the interaction of self-defocusing nonlinearity and Kerr nonlinearity.

Except for the $LiNbO_3$ waveguide, D. D. Hickstein et al. demonstrated the SCG using ALN waveguides with both cubic and quadratic nonlinearities.[239] The spectra of $TM_{00}$ mode showed the SHG, THG in the short wavelength and DFG in the long wavelength. X. Liu et al. used the chirp-modulated taper waveguide to realize the UV comb generators through the spectrum broadening.[140] The spectrum is extended to UV region via broad SHG and SFG.

## 7. Conclusion and Perspectives

We have presented a review of recent works on SCG in nanophotonic waveguides using various types of materials with three types of dispersion profiles, and analyzed the inherently physical mechanisms of different dispersion engineering techniques. From the perspective of the materials, the broadest SC is obtained by $Si_{0.2}Ge_{0.8}$ waveguide, whereas the deposit process need Ge fraction linearly increasing. The complex fabrication process could limit the extensive studies and applications. More representative experimental results are based on Si and $Si_3N_4$ platforms. One can see that Si waveguide is still the leading platform for nonlinear optics, even though having high TPA at telecommunication wavelengths. Meanwhile, $Si_3N_4$ is a particularly promising alternative nonlinear platform and has the great potential

for many key nonlinear applications. From the perspective of SCG method, pumping in the anomalous dispersion regime is still the mainstream method to obtain the SC due to the superiority in spectra broadening, which mainly depends on soliton fission and DW generation. Most spectra have obvious fluctuation and also have coherence degradation. The flatness of SC based on the dispersion with multiple ZDWs shows further improvement, but the method has not been experimentally demonstrated due to the following reason. The process of tailoring CD is very complex. Besides, the dispersion value and slope are very sensitive to the structure parameter variation. SCG with all-normal dispersion has the advantage of spectral flatness and high coherence. However, the corresponding limitation is the difficulty in achieving ultrabroadband SC spectra. Recent works are still focusing on numerical simulations and are lack of experimental demonstration. Even so, these chip-scale SCG works still provide the prospect of practical platforms for integrated nonlinear optics.

Overall, if we want to list the attractive potentials in the SCG research, the following aspects cannot be ignored. First, the SCG achieved in different materials could be used for different applications. Aside from the application of SC in the communications band toward optical communications systems, the SC spectrum covering the visible band is highly attractive for confocal microscopy,[234] label-free microscopy, and imaging in life sciences.[236,297] In the MIR regime, the molecules have strong rovibrational transitions, and it demonstrated the strong absorption coefficients for the hydrocarbons, nitrogen dioxide, greenhouse gases.[298–300] The SCs in the MIR band are widely applied for molecular spectroscopy,[41,301] health sensing,[302–304] and environmental monitoring,[305] which also attract lots of attentions. Second, some numerical works we discussed above with the promising dispersion engineering and broadband SCG could be further realized experimentally in the future. Additionally, a few other novel dispersion curves, that is, the most flattened, broadest, with the most ZDWs, could be extended further in the nonlinear optical applications. Advanced nanophotonic waveguides provide more degrees of freedom for dispersion engineering, and almost ideal dispersion profile for SCG could be obtained. Third, the novel materials with more pronounced Kerr nonlinearity provide an exciting arena for SCG or other nonlinear applications. The aforementioned novel material $TiO_2$[306] and others, such as hafnium dioxide ($HfO_2$),[307] gallium-nitride (GaN),[308,309] cadmium telluride (CdTe),[310] and PbO-$GeO_2$,[311] possess high third-order nonlinear susceptibilities. They require lower pump power and could be suitable for a broadband SCG. Most of these waveguides can be currently fabricated in the laboratory, whereas they are not the common and mature integrated optical platforms. The fabrication cost and period are the barriers for practical applications. In addition, they are still difficult to realize hybrid integration with CMOS-compatible materials. The hybrid waveguide[312] or high Kerr nonlinearity doped media[313] is also feasible to enhance the overall optical nonlinearity, thus it could be an ideal candidate for SCG. For example, the traditional SOI nanowire structure could be combined with the giant Kerr nonlinearity layered polymers,[131,314] Bragg grating,[315] and 2D materials[316] including graphene,[316,22,317] graphene oxide (GO),[318] black phosphorus,[319,320] and transition metal dichalcogenides,[321–324] which forms a hybrid structure to improve the performance of nonlinear integrated photonic devices. The fabrication procedures are more complex due to the additional structure. For instance, chemical vapor depositions-grown monolayer grapheme needs to be transferred on top of the Si waveguide, which should be conducted by precise positioning. The doped material like SiON[325,326] is the excellent platform for the design of nonlinear integrated photonic circuits with CMOS compatibility. Besides the conventional dielectric waveguides, plasmonics waveguide[327–329] with greatly enhanced light-matter interactions is predicted to be an exciting new platform for efficient Kerr nonlinear devices. Indeed, plasmonic waveguides can greatly enhance nonlinear effects through strong field confinement. However, nonlinear plasmonic devices still confront the challenges from the optical losses and material damage. Utilizing these novel platforms to generate broader SC is more effective and compact. In the coming decades, SC generated in novel material systems could enable new functionalities in numerous real applications. For instance, SC over multiple-octave range will lead to advances in frequency metrology, which could be seen as a "super long ruler" in the frequency domain to measure a random frequency. For sensing applications, ultra-broadband SC will expand the range of detectable analytes, and the output spectrum could have multiple features. Therefore, SC sources in new platforms have the possibilities to promote the development of biochemical sensing and imaging.

## Acknowledgements

This work was jointly supported by the National Key Research and Development Program of China (2019YFB1803700), the Key Technologies R & D Program of Tianjin (20YFZCGX00440), and the National Natural Science Foundation of China (NSFC) (11774181, 61775107, and 11874226).

## Conflict of Interest

The authors declare no conflict of interest.

## Keywords

integrated optics, nanophotonics, nonlinear optics, supercontinuum

Received: March 28, 2022
Revised: July 20, 2022
Published online: December 3, 2022

[1] A. Billat, D. Grassani, M. H. P. Pfeiffer, S. Kharitonov, T. J. Kippenberg, C. S. Bres, *Nat. Commun.* **2017**, *8*, 1016.
[2] P. A. Franken, A. E. Hill, C. W. Peters, G. Weinreich, *Phys. Rev. Lett.* **1961**, *7*, 118.
[3] A. M. Malvezzi, G. Vecchi, M. Patrini, G. Guizzetti, L. C. Andreani, F. Romanato, L. Businaro, E. Di Fabrizio, A. Passaseo, M. De Vittorio, *Phys. Rev. B* **2003**, *68*, 161306.
[4] M. P. Fischer, A. Riede, K. Gallacher, J. Frigerio, G. Pellegrini, M. Ortolani, D. J. Paul, G. Isella, A. Leitenstorfer, P. Biagioni, D. Brida, *Light: Sci. Appl.* **2018**, *7*, 106.
[5] C. C. Wang, J. Bomback, W. T. Donlon, C. R. Huo, J. James, *Phys. Rev. Lett.* **1986**, *57*, 1647.

[6] W. K. Burns, N. Bloembergen, *Phys. Rev. B* **1971**, *4*, 3437.
[7] J. S. Levy, M. A. Foster, A. L. Gaeta, M. Lipson, *Opt. Express* **2011**, *19*, 11415.
[8] Y.-Y. Lin, C.-L. Wu, W.-C. Chi, Y.-J. Chiu, Y.-J. Hung, A.-K. Chu, C.-K. Lee, *Opt. Express* **2016**, *24*, 21633.
[9] I.-W. Hsieh, X. Chen, J. I. Dadap, N. C. Panoiu, R. M. Osgoodr, S. J. McNab, Y. A. Vlasov, *Opt. Express* **2006**, *14*, 12380.
[10] X. Liu, J. B. Driscoll, J. I. Dadap, R. M. Osgood, S. Assefa, Y. A. Vlasov, W. M. J. Green, *Opt. Express* **2011**, *19*, 7778.
[11] E. Dulkeith, Y. A. Vlasov, X. Chen, N. C. Panoiu, R. M. Osgood, *Opt. Express* **2006**, *14*, 5524.
[12] P. Dumais, F. Gonthier, S. Lacroix, J. Bures, A. Villeneuve, P. G. J. Wigley, G. I. Stegeman, *Opt. Lett.* **1993**, *18*, 1996.
[13] I.-W. Hsieh, X. Chen, J. I. Dadap, N. C. Panoiu, R. M. Osgood, S. J. McNab, Y. A. Vlasov, *Opt. Express* **2007**, *15*, 1135.
[14] G. Genty, M. Lehtonen, H. Ludvigsen, *Opt. Express* **2004**, *12*, 4614.
[15] Ö. Boyraz, P. Koonath, V. Raghunathan, B. Jalali, *Opt. Express* **2004**, *12*, 4094.
[16] R. Claps, D. Dimitropoulos, V. Raghunathan, Y. Han, B. Jalali, *Opt. Express* **2003**, *11*, 1731.
[17] D. R. Solli, P. Koonath, B. Jalali, *Appl. Phys. Lett.* **2008**, *93*, 191105.
[18] V. Raghunathan, R. Claps, D. Dimitropoulos, B. Jalali, *Appl. Phys. Lett.* **2004**, *85*, 34.
[19] R. Claps, V. Raghunathan, D. Dimitropoulos, B. Jalali, *Opt. Express* **2004**, *12*, 2774.
[20] R. Claps, D. Dimitropoulos, Y. Han, B. Jalali, *Opt. Express* **2002**, *10*, 1305.
[21] Z. Wang, H. Liu, N. Huang, Q. Sun, J. Wen, *Opt. Express* **2012**, *20*, 8920.
[22] Y. Yang, Z. Xu, X. Jiang, Y. He, X. Guo, Y. Zhang, C. Qiu, Y. Su, *Photonics Res.* **2018**, *6*, 965.
[23] H. Fukuda, K. Yamada, T. Shoji, M. Takahashi, T. Tsuchizawa, T. Watanabe, J.-i. Takahashi, S.-i. Itabashi, *Opt. Express* **2005**, *13*, 4629.
[24] J. J. Wathen, P. Apiratikul, C. J. Richardson, G. A. Porkolab, G. M. Carter, T. E. Murphy, *Opt. Lett.* **2014**, *39*, 3161.
[25] Q. Lin, O. J. Painter, G. P. Agrawal, *Opt. Express* **2007**, *15*, 16604.
[26] M. A. Foster, A. C. Turner, M. Lipson, A. L. Gaeta, *Opt. Express* **2008**, *16*, 1300.
[27] H. Rong, Y.-H. Kuo, A. Liu, M. Paniccia, O. Cohen, *Opt. Express* **2006**, *14*, 1182.
[28] S. Zlatanovic, J. S. Park, S. Moro, J. M. C. Boggio, I. B. Divliansky, N. Alic, S. Mookherjea, S. Radic, *Nat. Photonics* **2010**, *4*, 561.
[29] Q. Lin, J. Zhang, P. M. Fauchet, G. P. Agrawal, *Opt. Express* **2006**, *14*, 4786.
[30] R. Dekker, A. Driessen, T. Wahlbrink, C. Moormann, J. Niehusmann, M. Först, *Opt. Express* **2006**, *14*, 8336.
[31] S. P. Stark, F. Biancalana, A. Podlipensky, P. S. J. Russell, *Phys. Rev. A* **2011**, *83*, 023808.
[32] M. A. Foster, A. C. Turner, J. E. Sharping, B. S. Schmidt, M. Lipson, A. L. Gaeta, *Nature* **2006**, *441*, 960.
[33] N. C. Panoiu, X. Chen, R. M. Osgood Jr., *Opt. Lett.* **2006**, *31*, 3609.
[34] B. Schenkel, R. Paschotta, U. Keller, *J. Opt. Soc. Am. B* **2005**, *22*, 687.
[35] C. Ciret, S.-P. Gorza, C. Husko, G. Roelkens, B. Kuyken, F. Leo, *Sci. Rep.* **2018**, *8*, 17177.
[36] J. Moses, F. W. Wise, *Opt. Lett.* **2006**, *31*, 1881.
[37] W. Tomlinson, R. Stolen, C. Shank, *J. Opt. Soc. Am. B* **1984**, *1*, 139.
[38] N. Singh, M. Xin, D. Vermeulen, K. Shtyrkova, N. Li, P. T. Callahan, E. S. Magden, A. Ruocco, N. Fahrenkopf, C. Baiocco, B. P. Kuo, S. Radic, E. Ippen, F. X. Kartner, M. R. Watts, *Light: Sci. Appl.* **2018**, *7*, 17131.
[39] H. Guo, C. Herkommer, A. Billat, D. Grassani, C. Zhang, M. H. P. Pfeiffer, W. Weng, C.-S. Brès, T. J. Kippenberg, *Nat. Photonics* **2018**, *12*, 330.
[40] E. S. Lamb, D. R. Carlson, D. D. Hickstein, J. R. Stone, S. A. Diddams, S. B. Papp, *Phys. Rev. Appl.* **2018**, *9*, 024030.
[41] A. Schliesser, N. Picqué, T. W. Hänsch, *Nat. Photonics* **2012**, *6*, 440.
[42] G. Agrawal, *Nonlinear Fiber Optics*, 3rd ed., Academic, New York **2001**.
[43] N. Nishizawa, Y. Chen, P. Hsiung, E. Ippen, J. Fujimoto, *Opt. Lett.* **2004**, *29*, 2846.
[44] I. Hartl, X. Li, C. Chudoba, R. Ghanta, T. Ko, J. Fujimoto, J. Ranka, R. Windeler, *Opt. Lett.* **2001**, *26*, 608.
[45] G. Humbert, W. Wadsworth, S. Leon-Saval, J. Knight, T. Birks, P. S. J. Russell, M. Lederer, D. Kopf, K. Wiesauer, E. Breuer, *Opt. Express* **2006**, *14*, 1596.
[46] W. Drexler, *J. Biomed. Opt.* **2004**, *9*, 47.
[47] D. R. Carlson, D. D. Hickstein, A. Lind, J. B. Olson, R. W. Fox, R. C. Brown, A. D. Ludlow, Q. Li, D. Westly, H. Leopardi, T. M. Fortier, K. Srinivasan, S. A. Diddams, S. B. Papp, *Phys. Rev. Appl.* **2017**, *8*, 014027.
[48] S. A. Diddams, L. Hollberg, V. Mbele, *Nature* **2007**, *445*, 627.
[49] C. R. Petersen, U. Møller, I. Kubat, B. Zhou, S. Dupont, J. Ramsay, T. Benson, S. Sujecki, N. Abdel-Moneim, Z. Tang, D. Furniss, A. Seddon, O. Bang, *Nat. Photonics* **2014**, *8*, 830.
[50] Y. Liu, M. D. King, H. Tu, Y. Zhao, S. A. Boppart, *Opt. Express* **2013**, *21*, 8269.
[51] M. K. Dasa, C. Markos, J. Janting, O. Bang, *J. Opt. Soc. Am. B* **2019**, *36*, A61.
[52] F. Yesilkoy, *Sensors* **2019**, *19*, 4287.
[53] M. Sieger, B. Mizaikoff, *Anal. Chem.* **2016**, *88*, 5562.
[54] Q. Du, Z. Luo, H. Zhong, Y. Zhang, Y. Huang, T. Du, W. Zhang, T. Gu, J. Hu, *Photonics Res.* **2018**, *6*, 506.
[55] B. Mizaikoff, *Chem. Soc. Rev.* **2013**, *42*, 8683.
[56] K. E. Jahromi, Q. Pan, L. Høgstedt, S. M. Friis, A. Khodabakhsh, P. M. Moselund, F. J. Harren, *Opt. Express* **2019**, *27*, 24469.
[57] Y. Luzinova, B. Zdyrko, I. Luzinov, B. Mizaikoff, *Anal. Chem.* **2012**, *84*, 1274.
[58] T. Nakasyotani, H. Toda, T. Kuri, K. Kitayama, *J. Lightwave Technol.* **2006**, *24*, 404.
[59] I. Zeylikovich, V. Kartazaev, R. Alfano, *J. Opt. Soc. Am. B* **2005**, *22*, 1453.
[60] T. Morioka, K. Mori, M. Saruwatari, *Electron. Lett.* **1993**, *29*, 862.
[61] T. Hakala, J. Suomalainen, S. Kaasalainen, Y. Chen, *Opt. Express* **2012**, *20*, 7119.
[62] J. M. Dudley, G. Genty, S. Coen, *Rev. Mod. Phys.* **2006**, *78*, 1135.
[63] R. R. Alfano, S. L. Shapiro, *Phys. Rev. Lett.* **1970**, *24*, 584.
[64] S. A. Diddams, D. J. Jones, J. Ye, S. T. Cundiff, J. L. Hall, J. K. Ranka, R. S. Windeler, R. Holzwarth, T. Udem, T. W. Hänsch, *Phys. Rev. Lett.* **2000**, *84*, 5102.
[65] X. Jiang, N. Y. Joly, M. A. Finger, F. Babic, M. Pang, R. Sopalla, M. H. Frosz, S. Poulain, M. Poulain, V. Cardin, J. C. Travers, P. S. J. Russell, *Opt. Lett.* **2016**, *41*, 4245.
[66] Q. Cao, X. Gu, E. Zeek, M. Kimmel, R. Trebino, J. Dudley, R. Windeler, *Appl. Phys. B: Lasers Opt.* **2003**, *77*, 239.
[67] K. L. Corwin, N. R. Newbury, J. M. Dudley, S. Coen, S. A. Diddams, K. Weber, R. Windeler, *Phys. Rev. Lett.* **2003**, *90*, 113904.
[68] M. Liao, X. Yan, G. Qin, C. Chaudhari, T. Suzuki, Y. Ohishi, *Opt. Express* **2009**, *17*, 15481.
[69] R. Zhang, J. Teipel, H. Giessen, *Opt. Express* **2006**, *14*, 6800.
[70] K. M. Hilligsøe, T. V. Andersen, H. N. Paulsen, C. K. Nielsen, K. Mølmer, S. Keiding, R. Kristiansen, K. P. Hansen, J. J. Larsen, *Opt. Express* **2004**, *12*, 1045.
[71] H. Ou, S. Dai, P. Zhang, Z. Liu, X. Wang, F. Chen, H. Xu, B. Luo, Y. Huang, R. Wang, *Opt. Lett.* **2016**, *41*, 3201.
[72] P. S. Westbrook, J. W. Nicholson, K. S. Feder, A. D. Yablon, *J. Lightwave Technol.* **2005**, *23*, 13.
[73] T. Hori, J. Takayanagi, N. Nishizawa, T. Goto, *Opt. Express* **2004**, *12*, 317.
[74] J. Leuthold, C. Koos, W. Freude, *Nat. Photonics* **2010**, *4*, 535.

[75] M. A. Foster, R. Salem, D. F. Geraghty, A. C. Turner-Foster, M. Lipson, A. L. Gaeta, *Nature* **2008**, *456*, 81.
[76] X. Liu, R. M. Osgood, Y. A. Vlasov, W. M. Green, *Nat. Photonics* **2010**, *4*, 557.
[77] M. Borghi, C. Castellan, S. Signorini, A. Trenti, L. Pavesi, *J. Opt.* **2017**, *19*, 093002.
[78] I. Avrutsky, R. Soref, *Opt. Express* **2011**, *19*, 21707.
[79] L. Zhang, A. M. Agarwal, L. C. Kimerling, J. Michel, *Nanophotonics* **2014**, *3*, 247.
[80] R. Soref, *Nat. Photonics* **2010**, *4*, 495.
[81] L. Shen, N. Healy, C. J. Mitchell, J. S. Penades, M. Nedeljkovic, G. Z. Mashanovich, A. C. Peacock, *Opt. Lett.* **2015**, *40*, 2213.
[82] F. De Leonardis, B. Troia, V. M. Passaro, *J. Lightwave Technol.* **2014**, *32*, 4349.
[83] L. Carletti, P. Ma, Y. Yu, B. Luther-Davies, D. Hudson, C. Monat, R. Orobtchouk, S. Madden, D. Moss, M. Brun, *Opt. Express* **2015**, *23*, 8261.
[84] K. Hammani, M. A. Ettabib, A. Bogris, A. Kapsalis, D. Syvridis, M. Brun, P. Labeye, S. Nicoletti, P. Petropoulos, *Opt. Express* **2014**, *22*, 9667.
[85] S. Serna, V. Vakarin, J.-M. Ramirez, J. Frigerio, A. Ballabio, X. Le Roux, L. Vivien, G. Isella, E. Cassan, N. Dubreuil, *Sci. Rep.* **2017**, *7*, 14692.
[86] K. Hammani, M. A. Ettabib, A. Bogris, A. Kapsalis, D. Syvridis, M. Brun, P. Labeye, S. Nicoletti, D. J. Richardson, P. Petropoulos, *Opt. Express* **2013**, *21*, 16690.
[87] D. J. Moss, R. Morandotti, A. L. Gaeta, M. Lipson, *Nat. Photonics* **2013**, *7*, 597.
[88] J. P. Epping, M. Hoekman, R. Mateman, A. Leinse, R. G. Heideman, A. van Rees, P. J. van der Slot, C. J. Lee, K.-J. Boller, *Opt. Express* **2015**, *23*, 642.
[89] M.-C. Tien, J. F. Bauters, M. J. Heck, D. J. Blumenthal, J. E. Bowers, *Opt. Express* **2010**, *18*, 23562.
[90] F. Gyger, J. Liu, F. Yang, J. He, A. S. Raja, R. N. Wang, S. A. Bhave, T. J. Kippenberg, L. Thévenaz, *Phys. Rev. Lett.* **2020**, *124*, 013902.
[91] E. Nitiss, O. Yakar, A. Stroganov, C.-S. Brès, *Opt. Lett.* **2020**, *45*, 1958.
[92] D. Tan, K. Ooi, D. Ng, *Photonics Res.* **2018**, *6*, B50.
[93] M. Ferrera, L. Razzari, D. Duchesne, R. Morandotti, Z. Yang, M. Liscidini, J. Sipe, S. Chu, B. Little, D. Moss, *Nat. Photonics* **2008**, *2*, 737.
[94] K. Ikeda, R. E. Saperstein, N. Alic, Y. Fainman, *Opt. Express* **2008**, *16*, 12987.
[95] D. Y. Oh, D. Sell, H. Lee, K. Y. Yang, S. A. Diddams, K. J. Vahala, *Opt. Lett.* **2014**, *39*, 1046.
[96] D. Duchesne, M. Ferrera, L. Razzari, R. Morandotti, B. E. Little, S. T. Chu, D. J. Moss, *Opt. Express* **2009**, *17*, 1865.
[97] A. Pasquazi, Y. Park, J. Azaña, F. Légaré, R. Morandotti, B. E. Little, S. T. Chu, D. J. Moss, *Opt. Express* **2010**, *18*, 7634.
[98] B. J. Eggleton, B. Luther-Davies, K. Richardson, *Nat. Photonics* **2011**, *5*, 141.
[99] M. Pelusi, F. Luan, S. Madden, D.-Y. Choi, D. Bulla, B. Luther-Davies, B. J. Eggleton, *IEEE Photonics Technol. Lett.* **2009**, *22*, 3.
[100] B. J. Eggleton, T. D. Vo, R. Pant, M. Pelusi, D. Y. Choi, S. Madden, B. Luther-Davies, *Laser Photonics Rev.* **2012**, *6*, 97.
[101] J. W. Choi, Z. Han, B.-U. Sohn, G. F. Chen, C. Smith, L. C. Kimerling, K. A. Richardson, A. M. Agarwal, D. T. Tan, *Sci. Rep.* **2016**, *6*, 39234.
[102] S. Madden, D.-Y. Choi, D. Bulla, A. V. Rode, B. Luther-Davies, V. G. Ta'eed, M. Pelusi, B. J. Eggleton, *Opt. Express* **2007**, *15*, 14414.
[103] V. G. Ta'eed, M. Shokooh-Saremi, L. Fu, I. C. Littler, D. J. Moss, M. Rochette, B. J. Eggleton, Y. Ruan, B. Luther-Davies, *IEEE J. Sel. Top. Quantum Electron.* **2006**, *12*, 360.
[104] M. Pu, L. Ottaviano, E. Semenova, K. Yvind, *Optica* **2016**, *3*, 823.
[105] U. D. Dave, B. Kuyken, F. Leo, S.-P. Gorza, S. Combrie, A. De Rossi, F. Raineri, G. Roelkens, *Opt. Express* **2015**, *23*, 4650.
[106] M. Savanier, C. Ozanam, L. Lanco, X. Lafosse, A. Andronico, I. Favero, S. Ducci, G. Leo, *Appl. Phys. Lett.* **2013**, *103*, 261105.
[107] K. Dolgaleva, W. C. Ng, L. Qian, J. S. Aitchison, *Opt. Express* **2011**, *19*, 12440.
[108] M. Jankowski, C. Langrock, B. Desiatov, A. Marandi, C. Wang, M. Zhang, C. R. Phillips, M. Lončar, M. Fejer, *Optica* **2020**, *7*, 40.
[109] R. Luo, Y. He, H. Liang, M. Li, Q. Lin, *Optica* **2018**, *5*, 1006.
[110] C. Wang, C. Langrock, A. Marandi, M. Jankowski, M. Zhang, B. Desiatov, M. M. Fejer, M. Lončar, *Optica* **2018**, *5*, 1438.
[111] K. Hammani, L. Markey, M. Lamy, B. Kibler, J. Arocas, J. Fatome, A. Dereux, J.-C. Weeber, C. Finot, *Appl. Sci.* **2018**, *8*, 543.
[112] R. Fan, C.-L. Wu, Y.-Y. Lin, C.-Y. Liu, P.-S. Hwang, C.-W. Liu, J. Qiao, M.-H. Shih, Y.-J. Hung, Y.-J. Chiu, *Opt. Lett.* **2019**, *44*, 1512.
[113] I. Babushkin, A. Husakou, J. Herrmann, Y. S. Kivshar, *Opt. Express* **2007**, *15*, 11978.
[114] U. D. Dave, S. Uvin, B. Kuyken, S. Selvaraja, F. Leo, G. Roelkens, *Opt. Express* **2013**, *21*, 32032.
[115] K. P. Yap, A. Delâge, J. Lapointe, B. Lamontagne, J. H. Schmid, P. Waldron, B. A. Syrett, S. Janz, *J. Lightwave Technol.* **2009**, *27*, 3999.
[116] T.-K. Liang, H. K. Tsang, *Appl. Phys. Lett.* **2004**, *84*, 2745.
[117] G. W. Rieger, K. S. Virk, J. F. Young, *Appl. Phys. Lett.* **2004**, *84*, 900.
[118] T.-K. Liang, H.-K. Tsang, *IEEE J. Sel. Top. Quantum Electron.* **2004**, *10*, 1149.
[119] R. Dekker, N. Usechak, M. Först, A. Driessen, *J. Phys. D: Appl. Phys.* **2007**, *40*, R249.
[120] C. Koos, L. Jacome, C. Poulton, J. Leuthold, W. Freude, *Opt. Express* **2007**, *15*, 5976.
[121] A. D. Bristow, N. Rotenberg, H. M. Van Driel, *Appl. Phys. Lett.* **2007**, *90*, 191104.
[122] H. K. Tsang, C. Wong, T. Liang, I. Day, S. Roberts, A. Harpin, J. Drake, M. Asghari, *Appl. Phys. Lett.* **2002**, *80*, 416.
[123] L. Yin, G. P. Agrawal, *Opt. Lett.* **2007**, *32*, 2031.
[124] T. Liang, H. Tsang, I. Day, J. Drake, A. Knights, M. Asghari, *Appl. Phys. Lett.* **2002**, *81*, 1323.
[125] N. Nader, D. L. Maser, F. C. Cruz, A. Kowligy, H. Timmers, J. Chiles, C. Fredrick, D. A. Westly, S. W. Nam, R. P. Mirin, *APL Photonics* **2018**, *3*, 036102.
[126] N. Singh, D. D. Hudson, B. J. Eggleton, *Opt. Express* **2015**, *23*, 17345.
[127] M. Zhu, H. Liu, X. Li, N. Huang, Q. Sun, J. Wen, Z. Wang, *Opt. Express* **2012**, *20*, 15899.
[128] L. Zhang, Q. Lin, Y. Yue, Y. Yan, R. G. Beausoleil, A. E. Willner, *Opt. Express* **2012**, *20*, 1685.
[129] L. Zhang, Q. Lin, Y. Yue, Y. Yan, R. G. Beausoleil, A. Agarwal, L. C. Kimerling, J. Michel, A. E. Willner, *IEEE J. Sel. Top. Quantum Electron.* **2012**, *18*, 1799.
[130] R. Sun, P. Dong, N.-n. Feng, C.-y. Hong, J. Michel, M. Lipson, L. Kimerling, *Opt. Express* **2007**, *15*, 17967.
[131] C. Koos, P. Vorreau, T. Vallaitis, P. Dumon, W. Bogaerts, R. Baets, B. Esembeson, I. Biaggio, T. Michinobu, F. Diederich, *Nat. Photonics* **2009**, *3*, 216.
[132] A. Martínez, J. Blasco, P. Sanchis, J. V. Galán, J. García-Rupérez, E. Jordana, P. Gautier, Y. Lebour, S. Hernández, R. Spano, *Nano Lett.* **2010**, *10*, 1506.
[133] P. Sanchis, J. Blasco, A. Martínez, J. Martí, *J. Lightwave Technol.* **2007**, *25*, 1298.
[134] C. A. Barrios, B. Sánchez, K. B. Gylfason, A. Griol, H. Sohlström, M. Holgado, R. Casquel, *Opt. Express* **2007**, *15*, 6846.
[135] Y. Guo, Z. Jafari, A. M. Agarwal, L. C. Kimerling, G. Li, J. Michel, L. Zhang, *Opt. Lett.* **2016**, *41*, 4939.
[136] S. Wang, J. Hu, H. Guo, X. Zeng, *Opt. Express* **2013**, *21*, 3067.
[137] L. Xu, M. Yang, Y. Guo, H. Liu, G. Li, L. Zhang, *J. Lightwave Technol.* **2019**, *37*, 6174.
[138] Y. Yue, L. Zhang, H. Huang, R. G. Beausoleil, A. E. Willner, *IEEE Photonics J.* **2011**, *4*, 126.
[139] S. Kasap, *Springer Handbook of Electronic and Photonic Materials*, Springer Science & Business Media, Southampton **2006**.

[140] X. Liu, A. W. Bruch, J. Lu, Z. Gong, J. B. Surya, L. Zhang, J. Wang, J. Yan, H. X. Tang, *Nat. Commun.* **2019**, *10*, 2971.
[141] P. T. Lin, H. Jung, L. C. Kimerling, A. Agarwal, H. X. Tang, *Laser Photonics Rev.* **2014**, *8*, L23.
[142] C. Xiong, W. H. Pernice, X. Sun, C. Schuck, K. Y. Fong, H. X. Tang, *New J. Phys.* **2012**, *14*, 095014.
[143] S. Mamoun, A. Merad, L. Guilbert, *Comput. Mater. Sci.* **2013**, *79*, 125.
[144] M. Leidinger, S. Fieberg, N. Waasem, F. Kühnemann, K. Buse, I. Breunig, *Opt. Express* **2015**, *23*, 21690.
[145] J. Lu, J. B. Surya, X. Liu, Y. Xu, H. X. Tang, *Opt. Lett.* **2019**, *44*, 1492.
[146] D. C. Harris, *Infrared Phys. Technol.* **1998**, *39*, 185.
[147] S. A. Miller, M. Yu, X. Ji, A. G. Griffith, J. Cardenas, A. L. Gaeta, M. Lipson, *Optica* **2017**, *4*, 707.
[148] S. Miyazaki, H. Nishimura, M. Fukuda, L. Ley, J. Ristein, *Appl. Surf. Sci.* **1997**, *113*, 585.
[149] A. L. Gaeta, M. Lipson, T. J. Kippenberg, *Nat. Photonics* **2019**, *13*, 158.
[150] R. A. Soref, S. J. Emelett, W. R. Buchwald, *J. Opt.* **2006**, *8*, 840.
[151] H. Lee, T. Chen, J. Li, O. Painter, K. J. Vahala, *Nat. Commun.* **2012**, *3*, 867.
[152] D. Tan, K. Ikeda, P. Sun, Y. Fainman, *Appl. Phys. Lett.* **2010**, *96*, 061101.
[153] J. F. Bauters, M. J. Heck, D. John, D. Dai, M.-C. Tien, J. S. Barton, A. Leinse, R. G. Heideman, D. J. Blumenthal, J. E. Bowers, *Opt. Express* **2011**, *19*, 3163.
[154] Y.-C. Chang, V. Paeder, L. Hvozdara, J.-M. Hartmann, H. P. Herzig, *Opt. Lett.* **2012**, *37*, 2883.
[155] J. M. Ramirez, V. Vakarin, C. Gilles, J. Frigerio, A. Ballabio, P. Chaisakul, X. L. Roux, C. Alonso-Ramos, G. Maisons, L. Vivien, *Opt. Lett.* **2017**, *42*, 105.
[156] J. M. Laniel, N. Hô, R. Vallée, A. Villeneuve, *J. Opt. Soc. Am. B* **2005**, *22*, 437.
[157] J. S. Sanghera, L. B. Shaw, I. D. Aggarwal, *C. R. Chim.* **2002**, *5*, 873.
[158] V. Shiryaev, M. Churbanov, *J. Non-Cryst. Solids* **2013**, *377*, 225.
[159] A. Prasad, C.-J. Zha, R.-P. Wang, A. Smith, S. Madden, B. Luther-Davies, *Opt. Express* **2008**, *16*, 2804.
[160] H. G. Dantanarayana, N. Abdel-Moneim, Z. Tang, L. Sojka, S. Sujecki, D. Furniss, A. B. Seddon, I. Kubat, O. Bang, T. M. Benson, *Opt. Mater. Express* **2014**, *4*, 1444.
[161] P. Ma, D.-Y. Choi, Y. Yu, X. Gai, Z. Yang, S. Debbarma, S. Madden, B. Luther-Davies, *Opt. Express* **2013**, *21*, 29927.
[162] J.-É. Tremblay, M. Malinowski, K. A. Richardson, S. Fathpour, M. C. Wu, *Opt. Express* **2018**, *26*, 21358.
[163] R. Ferrini, G. Guizzetti, M. Patrini, A. Parisini, L. Tarricone, B. Valenti, *Eur. Phys. J. B* **2002**, *27*, 449.
[164] L. Ottaviano, M. Pu, E. Semenova, K. Yvind, *Opt. Lett.* **2016**, *41*, 3996.
[165] Y. Bu, Z. Liu, L. Chen, Z. Cai, N. Chen, *Optoelectron. Adv. Mater., Rapid Commun.* **2010**, *4*, 1154.
[166] H. Zhang, B. Chen, J. F. Banfield, G. A. Waychunas, *Phys. Rev. B* **2008**, *78*, 214106.
[167] J. D. Bradley, C. C. Evans, J. T. Choy, O. Reshef, P. B. Deotare, F. Parsy, K. C. Phillips, M. Lončar, E. Mazur, *Opt. Express* **2012**, *20*, 23821.
[168] N. Cunha, A. Al-Rjoub, L. Rebouta, L. Vieira, S. Lanceros-Mendez, *Thin Solid Films* **2020**, *694*, 137736.
[169] M. Häyrinen, M. Roussey, V. Gandhi, P. Stenberg, A. Säynätjoki, L. Karvonen, M. Kuittinen, S. Honkanen, *J. Lightwave Technol.* **2013**, *32*, 208.
[170] C. Xiong, W. H. Pernice, H. X. Tang, *Nano Lett.* **2012**, *12*, 3562.
[171] W. H. Pernice, C. Xiong, H. X. Tang, *Opt. Express* **2012**, *20*, 12261.
[172] U. D. Dave, C. Ciret, S.-P. Gorza, S. Combrie, A. De Rossi, F. Raineri, G. Roelkens, B. Kuyken, *Opt. Lett.* **2015**, *40*, 3584.
[173] Y. Yu, X. Gai, P. Ma, D. Y. Choi, Z. Yang, R. Wang, S. Debbarma, S. J. Madden, B. Luther-Davies, *Laser Photonics Rev.* **2014**, *8*, 792.
[174] L. Petit, N. Carlie, H. Chen, S. Gaylord, J. Massera, G. Boudebs, J. Hu, A. Agarwal, L. Kimerling, K. Richardson, *J. Solid State Chem.* **2009**, *182*, 2756.
[175] E. D. Palik, *Handbook of Optical Constants of Solids*, Academic press, Maryland **1998**.
[176] I. H. Malitson, *J. Opt. Soc. Am.* **1965**, *55*, 1205.
[177] J. F. Bauters, M. J. Heck, D. D. John, J. S. Barton, C. M. Bruinink, A. Leinse, R. G. Heideman, D. J. Blumenthal, J. E. Bowers, *Opt. Express* **2011**, *19*, 24090.
[178] J. F. Bauters, M. L. Davenport, M. J. Heck, J. Doylend, A. Chen, A. W. Fang, J. E. Bowers, *Opt. Express* **2013**, *21*, 544.
[179] K. Wörhoff, R. G. Heideman, A. Leinse, M. Hoekman, *Adv. Opt. Technol.* **2015**, *4*, 189.
[180] H. Yamada, T. Chu, S. Ishida, Y. Arakawa, *IEEE J. Sel. Top. Quantum Electron.* **2006**, *12*, 1371.
[181] D. Duchesne, M. Peccianti, M. R. Lamont, M. Ferrera, L. Razzari, F. Légaré, R. Morandotti, S. Chu, B. E. Little, D. J. Moss, *Opt. Express* **2010**, *18*, 923.
[182] H. R. Philipp, *J. Electrochem. Soc.* **1973**, *120*, 295.
[183] J. Hong, A. M. Spring, F. Qiu, S. Yokoyama, *Sci. Rep.* **2019**, *9*, 12988.
[184] A. Gondarenko, J. S. Levy, M. Lipson, *Opt. Express* **2009**, *17*, 11366.
[185] C. G. Roeloffzen, L. Zhuang, C. Taddei, A. Leinse, R. G. Heideman, P. W. van Dijk, R. M. Oldenbeuving, D. A. Marpaung, M. Burla, K.-J. Boller, *Opt. Express* **2013**, *21*, 22937.
[186] A. Z. Subramanian, E. Ryckeboer, A. Dhakal, F. Peyskens, A. Malik, B. Kuyken, H. Zhao, S. Pathak, A. Ruocco, A. De Groote, *Photonics Res.* **2015**, *3*, B47.
[187] N. P. Barnes, M. S. Piltch, *J. Opt. Soc. Am.* **1979**, *69*, 178.
[188] W. S. Rodney, I. H. Malitson, T. A. King, *J. Opt. Soc. Am.* **1958**, *48*, 633.
[189] D. Aspnes, S. Kelso, R. Logan, R. Bhat, *J. Appl. Phys.* **1986**, *60*, 754.
[190] M. Schubert, V. Gottschalch, C. M. Herzinger, H. Yao, P. G. Snyder, J. A. Woollam, *J. Appl. Phys.* **1995**, *77*, 3416.
[191] N. K. Hon, R. Soref, B. Jalali, *J. Appl. Phys.* **2011**, *110*, 011301.
[192] R. Ganeev, A. Ryasnyansky, T. Usmanov, *Opt. Quantum Electron.* **2003**, *35*, 211.
[193] K. Ogusu, K. Shinkawa, *Opt. Express* **2009**, *17*, 8165.
[194] S. Combrié, Q. V. Tran, A. De Rossi, C. Husko, P. Colman, *Appl. Phys. Lett.* **2009**, *95*, 221108.
[195] A. Villeneuve, C. Yang, G. I. Stegeman, C. H. Lin, H. H. Lin, *Appl. Phys. Lett.* **1993**, *62*, 2465.
[196] F. Sanchez, G. Boudebs, S. Cherukulappurath, H. Leblond, J. Troles, F. Smektala, *J. Nonlinear Opt. Phys. Mater.* **2004**, *13*, 7.
[197] T. Mizunami, K. Takagi, *Opt. Lett.* **1994**, *19*, 463.
[198] G. Genty, S. Coen, J. M. Dudley, *J. Opt. Soc. Am. B* **2007**, *24*, 1771.
[199] M. H. Frosz, *Opt. Express* **2010**, *18*, 14778.
[200] A. R. Johnson, A. S. Mayer, A. Klenner, K. Luke, E. S. Lamb, M. R. Lamont, C. Joshi, Y. Okawachi, F. W. Wise, M. Lipson, *Opt. Lett.* **2015**, *40*, 5117.
[201] F. Leo, S.-P. Gorza, S. Coen, B. Kuyken, G. Roelkens, *Opt. Lett.* **2015**, *40*, 123.
[202] M. Bellini, T. W. Hänsch, *Opt. Lett.* **2000**, *25*, 1049.
[203] X. Gu, M. Kimmel, A. P. Shreenath, R. Trebino, J. M. Dudley, S. Coen, R. S. Windeler, *Opt. Express* **2003**, *11*, 2697.
[204] B. Kuyken, X. Liu, R. M. Osgood, R. Baets, G. Roelkens, W. M. Green, *Opt. Express* **2011**, *19*, 20172.
[205] R. K. Lau, M. R. Lamont, A. G. Griffith, Y. Okawachi, M. Lipson, A. L. Gaeta, *Opt. Lett.* **2014**, *39*, 4518.
[206] B. Kuyken, T. Ideguchi, S. Holzner, M. Yan, T. W. Hansch, J. Van Campenhout, P. Verheyen, S. Coen, F. Leo, R. Baets, G. Roelkens, N. Picque, *Nat. Commun.* **2015**, *6*, 6310.

[207] N. Singh, D. D. Hudson, Y. Yu, C. Grillet, S. D. Jackson, A. Casas-Bedoya, A. Read, P. Atanackovic, S. G. Duvall, S. Palomba, *Optica* **2015**, *2*, 797.
[208] T. Baehr-Jones, A. Spott, R. Ilic, A. Spott, B. Penkov, W. Asher, M. Hochberg, *Opt. Express* **2010**, *18*, 12127.
[209] R. Shankar, I. Bulu, M. Lončar, *Appl. Phys. Lett.* **2013**, *102*, 051108.
[210] A. Spott, Y. Liu, T. Baehr-Jones, R. Ilic, M. Hochberg, *Appl. Phys. Lett.* **2010**, *97*, 213501.
[211] F. Li, S. D. Jackson, C. Grillet, E. Magi, D. Hudson, S. J. Madden, Y. Moghe, C. O'Brien, A. Read, S. G. Duvall, *Opt. Express* **2011**, *19*, 15212.
[212] M. Sinobad, C. Monat, B. Luther-Davies, P. Ma, S. Madden, D. J. Moss, A. Mitchell, D. Allioux, R. Orobtchouk, S. Boutami, *Optica* **2018**, *5*, 360.
[213] M. Sinobad, A. D. Torre, B. Luther-Davis, P. Ma, S. Madden, S. Debbarma, K. Vu, D. J. Moss, A. Mitchell, J.-M. Hartmann, *J. Opt. Soc. Am. B* **2019**, *36*, A98.
[214] M. A. Ettabib, L. Xu, A. Bogris, A. Kapsalis, M. Belal, E. Lorent, P. Labeye, S. Nicoletti, K. Hammani, D. Syvridis, *Opt. Lett.* **2015**, *40*, 4118.
[215] A. G. Griffith, R. K. Lau, J. Cardenas, Y. Okawachi, A. Mohanty, R. Fain, Y. H. D. Lee, M. Yu, C. T. Phare, C. B. Poitras, *Nat. Commun.* **2015**, *6*, 6299.
[216] F. Leo, S.-P. Gorza, J. Safioui, P. Kockaert, S. Coen, U. Dave, B. Kuyken, G. Roelkens, *Opt. Lett.* **2014**, *39*, 3623.
[217] D. Carlson, D. Hickstein, A. Lind, J. Olson, R. Fox, R. Brown, A. Ludlow, Q. Li, D. Westly, H. Leopardi, *Phys. Rev. Appl.* **2017**, *8*, 014027
[218] F. De Leonardis, B. Troia, R. A. Soref, V. M. Passaro, *J. Lightwave Technol.* **2015**, *33*, 4437.
[219] A. Herzog, B. Hadad, V. Lyubin, M. Klebanov, A. Reiner, A. Shamir, A. A. Ishaaya, *Opt. Lett.* **2014**, *39*, 2522.
[220] M. Karim, B. Rahman, G. P. Agrawal, *Opt. Express* **2015**, *23*, 6903.
[221] M. Karim, B. Rahman, G. P. Agrawal, *Opt. Express* **2014**, *22*, 31029.
[222] A. Ishizawa, T. Goto, R. Kou, T. Tsuchizawa, N. Matsuda, K. Hitachi, T. Nishikawa, K. Yamada, T. Sogawa, H. Gotoh, *Appl. Phys. Lett.* **2017**, *111*, 021105.
[223] D. Martyshkin, V. Fedorov, T. Kesterson, S. Vasilyev, H. Guo, J. Liu, W. Weng, K. Vodopyanov, T. J. Kippenberg, S. Mirov, *Opt. Mater. Express* **2019**, *9*, 2553.
[224] A. Klenner, A. S. Mayer, A. R. Johnson, K. Luke, M. R. Lamont, Y. Okawachi, M. Lipson, A. L. Gaeta, U. Keller, *Opt. Express* **2016**, *24*, 11043.
[225] H. Saghaei, V. Van, *J. Opt. Soc. Am. B* **2019**, *36*, A193.
[226] N. Singh, M. Xin, D. Vermeulen, K. Shtyrkova, N. Li, P. T. Callahan, E. S. Magden, A. Ruocco, N. Fahrenkopf, C. Baiocco, *Light: Sci. Appl.* **2018**, *7*, 17131.
[227] M. R. Lamont, B. Luther-Davies, D.-Y. Choi, S. Madden, B. J. Eggleton, *Opt. Express* **2008**, *16*, 14938.
[228] X. Gai, D.-Y. Choi, S. Madden, Z. Yang, R. Wang, B. Luther-Davies, *Opt. Lett.* **2012**, *37*, 3870.
[229] Y. Yu, X. Gai, P. Ma, K. Vu, Z. Yang, R. Wang, D.-Y. Choi, S. Madden, B. Luther-Davies, *Opt. Lett.* **2016**, *41*, 958.
[230] T. S. Saini, U. K. Tiwari, R. K. Sinha, *J. Lightwave Technol.* **2018**, *36*, 1993.
[231] O. Fedotova, A. Husakou, J. Herrmann, *Opt. Express* **2006**, *14*, 1512.
[232] J. Yuan, Z. Kang, F. Li, X. Zhang, X. Sang, Q. Wu, B. Yan, K. Wang, X. Zhou, K. Zhong, *J. Lightwave Technol.* **2017**, *35*, 2994.
[233] R. Kou, T. Hatakeyama, J. Horng, J.-H. Kang, Y. Wang, X. Zhang, F. Wang, *Opt. Lett.* **2018**, *43*, 1387.
[234] H. Zhao, B. Kuyken, S. Clemmen, F. Leo, A. Subramanian, A. Dhakal, P. Helin, S. Severi, E. Brainis, G. Roelkens, *Opt. Lett.* **2015**, *40*, 2177.
[235] M. A. Porcel, F. Schepers, J. P. Epping, T. Hellwig, M. Hoekman, R. G. Heideman, P. J. van der Slot, C. J. Lee, R. Schmidt, R. Bratschitsch, *Opt. Express* **2017**, *25*, 1542.
[236] J. P. Epping, T. Hellwig, M. Hoekman, R. Mateman, A. Leinse, R. G. Heideman, A. van Rees, P. J. van der Slot, C. J. Lee, C. Fallnich, K. J. Boller, *Opt. Express* **2015**, *23*, 19596.
[237] M. Yu, B. Desiatov, Y. Okawachi, A. L. Gaeta, M. Lončar, *Opt. Lett.* **2019**, *44*, 1222.
[238] H. Chen, J. Zhou, D. Li, D. Chen, A. K. Vinod, H. Fu, X. Huang, T.-H. Yang, J. A. Montes, K. Fu, *ACS Photonics* **2021**, *8*, 1344.
[239] D. D. Hickstein, H. Jung, D. R. Carlson, A. Lind, I. Coddington, K. Srinivasan, G. G. Ycas, D. C. Cole, A. Kowligy, C. Fredrick, *Phys. Rev. Appl.* **2017**, *8*, 014025.
[240] L. Zhang, Y. Yan, Y. Yue, Q. Lin, O. Painter, R. G. Beausoleil, A. E. Willner, *Opt. Express* **2011**, *19*, 11584.
[241] H. Ryu, J. Kim, Y. M. Jhon, S. Lee, N. Park, *Opt. Express* **2012**, *20*, 13189.
[242] C. Bao, Y. Yan, L. Zhang, Y. Yue, N. Ahmed, A. M. Agarwal, L. C. Kimerling, J. Michel, A. E. Willner, *J. Opt. Soc. Am. B* **2015**, *32*, 26.
[243] C. G. Roeloffzen, M. Hoekman, E. J. Klein, L. S. Wevers, R. B. Timens, D. Marchenko, D. Geskus, R. Dekker, A. Alippi, R. Grootjans, *IEEE J. Sel. Top. Quantum Electron.* **2018**, *24*, 4400321.
[244] Y. Fang, C. Bao, Z. Wang, B. Liu, L. Zhang, X. Han, Y. He, H. Huang, Y. Ren, Z. Pan, *J. Lightwave Technol.* **2020**, *38*, 3431.
[245] L. Zhang, Y. Yue, Y. Xiao-Li, R. G. Beausoleil, A. E. Willner, *Opt. Express* **2009**, *17*, 7095.
[246] L. Zhang, Y. Yue, R. G. Beausoleil, A. E. Willner, *Opt. Express* **2010**, *18*, 20529.
[247] Z. Jafari, F. Emami, *Opt. Lett.* **2013**, *38*, 3082.
[248] Y. Guo, Z. Jafari, L. Xu, C. Bao, P. Liao, G. Li, A. M. Agarwal, L. C. Kimerling, J. Michel, A. E. Willner, *Photonics Res.* **2019**, *7*, 1279.
[249] N. Singh, D. Vermulen, A. Ruocco, N. Li, E. Ippen, F. X. Kärtner, M. R. Watts, *Opt. Express* **2019**, *27*, 31698.
[250] A. R. Johnson, X. Ji, M. R. Lamont, Y. Okawachi, M. Lipson, A. L. Gaeta, *Coherent Supercontinuum Generation with Picosecond Pulses, CLEO: Science and Innovations*, Optical Society of America, **2017**, pp. SF1C. 3.
[251] C. Ciret, S.-P. Gorza, *J. Opt. Soc. Am. B* **2017**, *34*, 1156.
[252] J. Wei, C. Ciret, M. Billet, F. Leo, B. Kuyken, S.-P. Gorza, *Phys. Rev. Appl.* **2020**, *14*, 054045.
[253] E. Sahin, A. Blanco-Redondo, B.-U. Sohn, Y. Cao, G. F. Chen, D. K. Ng, B. J. Eggleton, D. T. Tan, *Adv. Photonics Res.* **2021**, *2*, 2100107.
[254] C. Phillips, C. Langrock, J. Pelc, M. Fejer, J. Jiang, M. E. Fermann, I. Hartl, *Opt. Lett.* **2011**, *36*, 3912.
[255] D. D. Hickstein, G. C. Kerber, D. R. Carlson, L. Chang, D. Westly, K. Srinivasan, A. Kowligy, J. E. Bowers, S. A. Diddams, S. B. Papp, *Phys. Rev. Lett.* **2018**, *120*, 053903.
[256] E. Kelleher, M. Erkintalo, J. Travers, *Opt. Lett.* **2012**, *37*, 5217.
[257] J. M. Dudley, S. Coen, *IEEE J. Sel. Top. Quantum Electron.* **2002**, *8*, 651.
[258] J. M. Dudley, S. Coen, *Opt. Lett.* **2002**, *27*, 1180.
[259] A. Demircan, U. Bandelow, *Appl. Phys. B: Lasers Opt.* **2007**, *86*, 31.
[260] G. Genty, M. Surakka, J. Turunen, A. T. Friberg, *J. Opt. Soc. Am. B* **2011**, *28*, 2301.
[261] J. Safioui, F. Leo, B. Kuyken, S.-P. Gorza, S. K. Selvaraja, R. Baets, P. Emplit, G. Roelkens, S. Massar, *Opt. Express* **2014**, *22*, 3089.
[262] A. Mussot, E. Lantz, H. Maillotte, T. Sylvestre, C. Finot, S. Pitois, *Opt. Express* **2004**, *12*, 2838.
[263] J. M. Dudley, G. Genty, F. Dias, B. Kibler, N. Akhmediev, *Opt. Express* **2009**, *17*, 21497.
[264] D. Grassani, E. Tagkoudi, H. Guo, C. Herkommer, F. Yang, T. J. Kippenberg, C.-S. Brès, *Nat. Commun.* **2019**, *10*, 1553.
[265] A. D. Torre, M. Sinobad, R. Armand, B. Luther-Davies, P. Ma, S. Madden, A. Mitchell, D. J. Moss, J.-M. Hartmann, V. Reboud, *APL Photonics* **2021**, *6*, 016102.
[266] M. Montesinos-Ballester, C. Lafforgue, J. Frigerio, A. Ballabio, V. Vakarin, Q. Liu, J. M. Ramirez, X. L. Roux, D. Bouville, A. Barzaghi, *ACS Photonics* **2020**, *7*, 3423.

[267] B. Kuyken, M. Billet, F. Leo, K. Yvind, M. Pu, *Opt. Lett.* **2020**, *45*, 603.
[268] F. Leo, J. Safioui, B. Kuyken, G. Roelkens, S.-P. Gorza, *Opt. Express* **2014**, *22*, 28997.
[269] K. F. Lamee, D. R. Carlson, Z. L. Newman, S.-P. Yu, S. B. Papp, *Opt. Lett.* **2020**, *45*, 4192.
[270] Y. Okawachi, M. Yu, J. Cardenas, X. Ji, M. Lipson, A. L. Gaeta, *Opt. Lett.* **2017**, *42*, 4466.
[271] I.-W. Hsieh, X. Chen, X. Liu, J. I. Dadap, N. C. Panoiu, C.-Y. Chou, F. Xia, W. M. Green, Y. A. Vlasov, R. M. Osgood, *Opt. Express* **2007**, *15*, 15242.
[272] L. Yin, Q. Lin, G. P. Agrawal, *Opt. Lett.* **2007**, *32*, 391.
[273] J. Hwang, D.-G. Kim, S. Han, D. Jeong, Y.-H. Lee, D.-Y. Choi, H. Lee, *Opt. Lett.* **2021**, *46*, 2413.
[274] R. Halir, Y. Okawachi, J. Levy, M. Foster, M. Lipson, A. Gaeta, *Opt. Lett.* **2012**, *37*, 1685.
[275] A. Mayer, A. Klenner, A. Johnson, K. Luke, M. Lamont, Y. Okawachi, M. Lipson, A. Gaeta, U. Keller, *Opt. Express* **2015**, *23*, 15440.
[276] Y. Okawachi, M. Yu, J. Cardenas, X. Ji, A. Klenner, M. Lipson, A. L. Gaeta, *Opt. Lett.* **2018**, *43*, 4627.
[277] T. Wang, D. K. Ng, S. K. Ng, Y. T. Toh, A. K. Chee, G. F. Chen, Q. Wang, D. T. Tan, *Laser Photonics Rev.* **2015**, *9*, 498.
[278] C. Lafforgue, S. Guerber, J. M. Ramirez, G. Marcaud, C. Alonso-Ramos, X. L. Roux, D. Marris-Morini, E. Cassan, C. Baudot, F. Boeuf, *Photonics Res.* **2020**, *8*, 352.
[279] Y. Cao, B.-U. Sohn, H. Gao, P. Xing, G. F. Chen, D. K. Ng, D. T. Tan, *Sci. Rep.* **2022**, *12*, 9487.
[280] D. Y. Oh, K. Y. Yang, C. Fredrick, G. Ycas, S. A. Diddams, K. J. Vahala, *Nat. Commun.* **2017**, *8*, 13922.
[281] H. Shang, D. Sun, M. Zhang, J. Song, Z. Yang, D. Liu, S. Zeng, L. Wan, B. Zhang, Z. Wang, *J. Lightwave Technol.* **2021**, *39*, 3890.
[282] J. R. Woods, J. Daykin, A. S. Tong, C. Lacava, P. Petropoulos, A. C. Tropper, P. Horak, J. S. Wilkinson, V. Apostolopoulos, *Opt. Express* **2020**, *28*, 32173.
[283] S. S. Bobba, A. Agrawal, *Sci. Rep.* **2017**, *7*, 10192.
[284] J. Lu, X. Liu, A. W. Bruch, L. Zhang, J. Wang, J. Yan, H. X. Tang, *Opt. Lett.* **2020**, *45*, 4499.
[285] C. Lafforgue, M. Montesinos-Ballester, X. L. Roux, E. Cassan, D. Marris-Morini, C. Alonso-Ramos, L. Vivien, *Photonics Res.* **2022**, *10*, A43.
[286] C. Finot, B. Kibler, L. Provost, S. Wabnitz, *J. Opt. Soc. Am. B* **2008**, *25*, 1938.
[287] M. Sinobad, A. DellaTorre, R. Armand, B. Luther-Davies, P. Ma, S. Madden, A. Mitchell, D. J. Moss, J.-M. Hartmann, J.-M. Fedeli, *Opt. Lett.* **2020**, *45*, 5008.
[288] E. Tagkoudi, C. G. Amiot, G. Genty, C.-S. Brès, *Opt. Express* **2021**, *29*, 21348.
[289] M. Yang, Y. Guo, J. Wang, Z. Han, K. Wada, L. C. Kimerling, A. M. Agarwal, J. Michel, G. Li, L. Zhang, *Opt. Express* **2017**, *25*, 16116.
[290] R. DeSalvo, D. J. Hagan, M. Sheik-Bahae, G. Stegeman, E. W. Van Stryland, H. Vanherzeele, *Opt. Lett.* **1992**, *17*, 28.
[291] M. Sundheimer, C. Bosshard, E. Van Stryland, G. Stegeman, J. Bierlein, *Opt. Lett.* **1993**, *18*, 1397.
[292] C. Langrock, M. Fejer, I. Hartl, M. E. Fermann, *Opt. Lett.* **2007**, *32*, 2478.
[293] H. Guo, B. Zhou, M. Steinert, F. Setzpfandt, T. Pertsch, H.-p. Chung, Y.-H. Chen, M. Bache, *Opt. Lett.* **2015**, *40*, 629.
[294] H. Guo, X. Zeng, B. Zhou, M. Bache, *Opt. Lett.* **2014**, *39*, 1105.
[295] C. Phillips, C. Langrock, J. Pelc, M. Fejer, I. Hartl, M. E. Fermann, *Opt. Express* **2011**, *19*, 18754.
[296] H. Guo, B. Zhou, X. Zeng, M. Bache, *Opt. Express* **2014**, *22*, 12211.
[297] J. P. Epping, M. Kues, P. J. van der Slot, C. J. Lee, C. Fallnich, K.-J. Boller, *Opt. Express* **2013**, *21*, 32123.
[298] E. Baumann, F. R. Giorgetta, W. C. Swann, A. M. Zolot, I. Coddington, N. R. Newbury, *Phys. Rev. A* **2011**, *84*, 062513.
[299] B. J. Bjork, T. Q. Bui, O. H. Heckl, P. B. Changala, B. Spaun, P. Heu, D. Follman, C. Deutsch, G. D. Cole, M. Aspelmeyer, *Science* **2016**, *354*, 444.
[300] L. Zhu, D. J. Jacob, P. S. Kim, J. A. Fisher, K. Yu, K. R. Travis, L. J. Mickley, R. M. Yantosca, M. P. Sulprizio, I. De Smedt, *Atmos. Chem. Phys.* **2016**, *16*, 13477.
[301] A. J. Lind, A. Kowligy, H. Timmers, F. C. Cruz, N. Nader, M. C. Silfies, T. K. Allison, S. A. Diddams, *Phys. Rev. Lett.* **2020**, *124*, 133904.
[302] G. Clemens, J. R. Hands, K. M. Dorling, M. J. Baker, *Analyst* **2014**, *139*, 4411.
[303] M. J. Walsh, R. K. Reddy, R. Bhargava, *IEEE J. Sel. Top. Quantum Electron.* **2012**, *18*, 1502.
[304] K. Maquelin, C. Kirschner, L.-P. Choo-Smith, N. van den Braak, H. P. Endtz, D. Naumann, G. Puppels, *J. Microbiol. Methods* **2002**, *51*, 255.
[305] E. Tagkoudi, D. Grassani, F. Yang, C. Herkommer, T. Kippenberg, C.-S. Brès, *Opt. Lett.* **2020**, *45*, 2195.
[306] R. Luo, Y. He, H. Liang, M. Li, Q. Lin, *Laser Photonics Rev.* **2019**, *13*, 1800288.
[307] S.-S. Lin, H.-R. Li, *Ceram. Int.* **2013**, *39*, 7677.
[308] E. Stassen, M. Pu, E. Semenova, E. Zavarin, W. Lundin, K. Yvind, *Opt. Lett.* **2019**, *44*, 1064.
[309] Y. Zheng, C. Sun, B. Xiong, L. Wang, Z. Hao, J. Wang, Y. Han, H. Li, J. Yu, Y. Luo, *Laser Photonics Rev.* **2022**, *16*, 2100071.
[310] Z. Long, H. Yang, Y. Li, H. Wu, H. Liang, *Opt. Express* **2022**, *30*, 2265.
[311] L. A. Gómez, F. dos Santos, A. Gomes, C. B. de Araújo, L. R. Kassab, W. G. Hora, *Appl. Phys. Lett.* **2008**, *92*, 141916.
[312] F. Eltes, D. Caimi, F. Fallegger, M. Sousa, E. O'Connor, M. D. Rossell, B. Offrein, J. Fompeyrine, S. Abel, *ACS Photonics* **2016**, *3*, 1698.
[313] S. Zenkin, F. Konusov, A. Lauk, D. Zelentsov, S. Demchenko, *Coatings* **2019**, *9*, 53.
[314] T. Vallaitis, S. Bogatscher, L. Alloatti, P. Dumon, R. Baets, M. L. Scimeca, I. Biaggio, F. Diederich, C. Koos, W. Freude, *Opt. Express* **2009**, *17*, 17357.
[315] N. Singh, M. Raval, E. Ippen, M. R. Watts, F. X. Kärtner, *Appl. Phys. Lett.* **2021**, *118*, 071106.
[316] Q. Feng, H. Cong, B. Zhang, W. Wei, Y. Liang, S. Fang, T. Wang, J. Zhang, *Appl. Phys. Lett.* **2019**, *114*, 071104.
[317] Q. Jin, X. Li, J. Chen, S. Gao, *Sci. Rep.* **2017**, *7*, 12290.
[318] Y. Zhang, J. Wu, Y. Yang, Y. Qu, L. Jia, T. Moein, B. Jia, D. J. Moss, *ACS Appl. Mater. Interfaces* **2020**, *12*, 33094.
[319] S. Lu, L. Miao, Z. Guo, X. Qi, C. Zhao, H. Zhang, S. Wen, D. Tang, D. Fan, *Opt. Express* **2015**, *23*, 11183.
[320] Y. Xu, X.-F. Jiang, Y. Ge, Z. Guo, Z. Zeng, Q.-H. Xu, H. Zhang, X.-F. Yu, D. Fan, *J. Mater. Chem. C* **2017**, *5*, 3007.
[321] S. Manzeli, D. Ovchinnikov, D. Pasquier, O. V. Yazyev, A. Kis, *Nat. Rev. Mater.* **2017**, *2*, 17033.
[322] Q. H. Wang, K. Kalantar-Zadeh, A. Kis, J. N. Coleman, M. S. Strano, *Nat. Nanotechnol.* **2012**, *7*, 699.
[323] C. Janisch, Y. Wang, D. Ma, N. Mehta, A. L. Elías, N. Perea-López, M. Terrones, V. Crespi, Z. Liu, *Sci. Rep.* **2014**, *4*, 5530.
[324] A. Säynätjoki, L. Karvonen, H. Rostami, A. Autere, S. Mehravar, A. Lombardo, R. A. Norwood, T. Hasan, N. Peyghambarian, H. Lipsanen, *Nat. Commun.* **2017**, *8*, 893.
[325] R. Germann, H. Salemink, R. Beyeler, G. Bona, F. Horst, I. Massarek, B. Offrein, *J. Electrochem. Soc.* **2000**, *147*, 2237.
[326] K. Wörhoff, L. Hilderink, A. Driessen, P. Lambeck, *J. Electrochem. Soc.* **2002**, *149*, F85.
[327] G. Li, C. M. de Sterke, S. Palomba, *Laser Photonics Rev.* **2016**, *10*, 639.
[328] G. Li, C. M. De Sterke, S. Palomba, *ACS Photonics* **2018**, *5*, 1034.
[329] M. P. Fischer, A. Riede, K. Gallacher, J. Frigerio, G. Pellegrini, M. Ortolani, D. J. Paul, G. Isella, A. Leitenstorfer, P. Biagioni, *Light: Sci. Appl.* **2018**, *7*, 106.

**Yuxi Fang** received her B.S. degree in optical information science and technology from Anhui University, Hefei, Anhui, China, in 2018. She is currently a doctoral student at Nankai University in China, and also a visiting student at Ghent University in Belgium. Her research interest includes integrated photonics and nonlinear optics. She has authored and coauthored 60 research papers, including 26 journal articles and 34 conference proceedings, 1 patent, and 1 book chapter. She is also a student ember of IEEE and OSA.

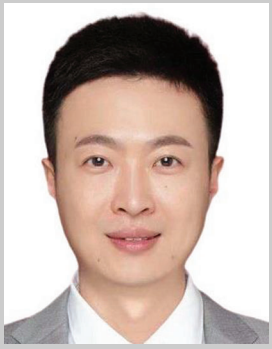

**Yang Yue** is a Professor with the School of Information and Communications Engineering, Xi'an Jiaotong University, China. Dr. Yue's current research interest is intelligent photonics, including optical communications, optical perception, and optical chip. He has published over 200 journal papers (including Science) and conference proceedings with >10,000 citations, five edited books, two book chapters, >50 issued or pending patents. Dr. Yue is a Senior Member of IEEE, Optica and SPIE. He is an Associate Editor for IEEE Access and Frontiers in Physics, Editor Board Member for four other scientific journals, Guest Editor for >10 journal special issues.